

Lattice Distortion in a Zircon Population and its Effects on Trace Element Mobility and U-Th-Pb Isotope Systematics: Examples from the Lewisian Gneiss Complex, Northwest Scotland

John M. MacDonald¹, John Wheeler¹, Simon L. Harley², Elisabetta Mariani¹, Kathryn M. Goodenough³, Quentin Crowley⁴, Daniel Tatham¹

¹ School of Environmental Sciences, Jane Herdman Laboratories, University of Liverpool, L69 3GP, UK
² School of GeoSciences, Grant Institute, The King’s Buildings, West Mains Road, Edinburgh, EH9 3JW, UK
³ British Geological Survey, Murchison House, West Mains Road, Edinburgh, EH9 3LA, UK
⁴ Dept. Geology, School of Natural Sciences, Trinity College, Dublin 2, Ireland, IE

Corresponding author: John M. MacDonald
Postal: School of Environmental Sciences, University of Liverpool, L69 3GP, UK.
Email: jmacd@liv.ac.uk
Telephone: 01517945201

Abstract Zircon is a key mineral in geochemical and geochronological studies in a range of geological settings as it is mechanically and chemically robust. However, distortion of its crystal lattice can facilitate enhanced diffusion of key elements such as U and Pb. Electron Backscatter Diffraction (EBSD) analysis of ninety-nine zircons from the Lewisian Gneiss Complex (LGC) of northwest Scotland has revealed five zircons with lattice distortion. The distortion can take the form of gradual bending of the lattice or division of the crystal into subgrains. Zircon lattices are distorted because of either post-crystallisation plastic distortion or growth defects. Three of the five distorted zircons, along with many of the undistorted zircons in the population, were analysed by ion

microprobe to measure U and Pb isotopes, Ti and REEs. Comparison of Th/U ratio, $^{207}\text{Pb}/^{206}\text{Pb}$ age, REE profile and Ti concentration between zircons with and without lattice distortion suggests that the distortion is variably affecting the concentration of these trace elements and isotopes within single crystals, within samples and between localities. REE patterns vary heterogeneously, sometimes relatively depleted in heavy REEs or lacking a Eu anomaly. Ti-in-zircon thermometry records temperatures that were either low ($\sim 700^\circ\text{C}$) or high ($>900^\circ\text{C}$) relative to undistorted zircons. One distorted zircon records apparent $^{207}\text{Pb}/^{206}\text{Pb}$ isotopic ages (-3.0% to +0.3% discordance) in the range of $\sim 2420\text{--}2450\text{Ma}$ but this does not correlate with any previously dated tectonothermal event in the LGC. Two other distorted zircons give discordant ages of $2331\pm 22\text{Ma}$ and $2266\pm 0\text{Ma}$, defining a discordia lower intercept within error of a late amphibolite-facies tectonothermal event. This illustrates that Pb may be mobilised in distorted zircons at lower metamorphic grade than in undistorted zircons. These differences in trace element abundances and isotope systematics in distorted zircons relative to undistorted zircons are generally interpreted to have been facilitated by subgrain walls. Trace elements and isotopes would have moved from undistorted lattice into these subgrain walls as their chemical potential is modified due to the presence of the dislocations which make up the subgrain wall. Subgrain walls provided pathways for chemical exchange between crystal and surroundings. Only five per cent of zircons in this population have lattice distortion suggesting it will not have a major impact on zircon geochronology studies, particularly as three of the five distorted zircons are from strongly deformed rocks not normally sampled in such studies. However, this does suggest there may be a case for EBSD analysis of zircons prior to geochemical analysis when zircons from highly deformed rocks are to be investigated.

Keywords – zircon, lattice distortion, trace elements & isotopes, EBSD

Introduction

Zircon is a common accessory mineral in a wide range of sedimentary, igneous and metamorphic rocks. It has a high volume diffusion closure temperature of typically >900°C for radiogenic Pb (Cherniak and Watson, 2003) and is regarded as a mechanically and chemically robust mineral (Finch and Hanchar, 2003), suitable for geochemical investigation of Precambrian geological events. The primary incorporation of uranium but not lead makes it ideal for radiometric dating; it also contains other elements such as hafnium, titanium and the rare earth elements (REE), which allow a range of geological interpretations to be made.

Populations of zircons are routinely analysed to determine the tectonothermal evolution of rocks throughout the world, generally involving U-Pb isotopic measurements. Recent research, however, has indicated that some of this isotopic and trace element analysis could be compromised by plastic deformation of the zircon crystal lattice (Reddy et al., 2006; Timms et al., 2006a; Timms et al., 2006b; Timms et al., 2011; Piazzolo et al., 2012). Plastic deformation occurs when forces applied to a grain cause the crystal lattice to bend and distort through movement of lattice dislocations; crystals may also grow with defects and therefore have a distorted lattice from the time of their initial formation. High spatial resolution zircon analysis has conventionally been guided by backscattered electron (BSE) and cathodoluminescence (CL) imaging in a scanning electron microscope. CL reveals internal chemical zoning, xenocrysts, overgrowths, inclusions and metamictisation while BSE imaging highlights fractures. Fractures are generally avoided in subsequent analysis as they may contain contamination or may have lost or gained key elements, which would result in data giving meaningless geological interpretations. While BSE and CL can show brittle deformation (fracturing) of the crystal lattice, they do not show plastic lattice distortion.

The technique required to reveal lattice distortion is electron backscatter diffraction (EBSD) (Prior et al., 1999; Prior et al., 2009). EBSD mapping is conducted inside a scanning electron microscope. The electron beam rasters across the sample surface and at each point a Kikuchi (diffraction) pattern is obtained. EBSD software automatically indexes prominent lattice planes from the diffraction pattern, which are controlled by the crystal lattice orientation (Prior et al., 1999). If

there is variation in the crystallographic orientation across a crystal (lattice distortion), this will be shown by an EBSD map.

Reddy et al. (2006) first showed that lattice distortion, in the form of low-angle boundaries from the plastic deformation of zircon, acted as enhanced diffusion pathways for trace elements. CL imaging of a single zircon megacryst from an Indian Ocean gabbro revealed narrow lines of reduced CL emittance, corresponding with the low-angle boundaries highlighted by EBSD analysis. Ion microprobe analysis of REEs indicated that in the part of the megacryst that had been plastically deformed, REE abundance had been modified from that in the undeformed part; REE patterns showed a relative enrichment in middle REEs and depletion in heavy REEs.

Timms et al. (2006b) investigated the effects of lattice distortion formed by plastic deformation on the U-Th-Pb system in a zircon megacryst from the Lewisian Gneiss Complex (LGC) of Northwest Scotland (the same host rocks as the zircon population in this study). They found that, as with REEs, low-angle boundaries within the zircon megacryst acted as enhanced diffusion pathways for U and Th; the highest measured concentrations and Th/U ratios were found to be in these microstructures. $^{207}\text{Pb}/^{206}\text{Pb}$ ages were uniform across the megacryst, which led the authors to infer that plastic deformation had occurred shortly after crystallisation.

Timms et al. (2011) examined another zircon megacryst, this time from a Siberian xenolith. As with the zircons from the LGC and Indian Ocean, this megacryst contained subgrains separated by low-angle boundaries. They determined that Ti is also affected by lattice distortion, as with REE and U-Th-Pb in their previous studies. The low-angle boundaries were depleted in Ti relative to the subgrains and this could not be explained by volume diffusion alone – the low-angle boundaries were acting as fast diffusion pathways.

Piazolo et al. (2012) investigated plastic lattice distortion in two large zircon porphyroclasts of 0.8-1.5mm size and associated aggregated grains. They recorded rotations around $\langle 001 \rangle$, highly distorted half-circular shaped deformation zones located at grain edges, and low-angle boundary

networks forming deformation zones up to 100 μm wide. CL patterns and U-Pb ages were found to have been variably reset by the lattice distortions.

This previous work documented examples of plastic deformation in single zircon megacrysts several millimetres in diameter, mainly hosted in undeformed rocks. In this contribution we investigate the frequency, effects and causes of plastic deformation across a large population of zircons of more normal size ($<200\mu\text{m}$ length), of the type routinely used for U-Pb dating and other geochemical analysis, from rocks with varying degrees of deformation. Our multigrain study comprises ninety-nine zircons, all of which we have analysed by EBSD. A subset of zircons with and without lattice distortion were analysed by ion microprobe for U-Th-Pb, REE and Ti and we document the effect of the lattice distortion on the mobility of these elements and isotopes. We also investigate the relationship between the frequency of lattice distortion and deformation in the host rock, and speculate on the causes of the lattice distortion.

Geological Setting

Rocks from the Lewisian Gneiss Complex (LGC) of northwest Scotland were chosen for this study. The LGC crops out along the coastal strip of the northwest mainland as well as most of the Outer Hebrides (Fig. 1a). The LGC is composed dominantly of tonalite-trondhjemite-granodiorite (TTG) gneisses with subordinate mafic and metasedimentary units, cross-cut by the mafic Scourie Dyke Swarm and minor granite and pegmatite sheets (e.g. Peach et al., 1907; Tarney and Weaver, 1987). Sutton and Watson (1951) distinguished two tectonothermal events, one before and one after intrusion of the Scourie Dykes; the later of these two events, the Laxfordian, comprised static and dynamic amphibolite-facies retrogression and heterogeneous deformation across the LGC. Sutton and Watson named the pre-Scourie dyke event the 'Scourian' but it has since been subdivided into the Badcallian (Park, 1970) and the Inverian (Evans, 1965). Both the Badcallian and Inverian are heterogeneously overprinted by the Laxfordian and are only preserved in certain areas of the complex, most notably the 'Central Region' of Sutton and Watson (1951), the area around

Scourie (Fig. 5.1b). Field mapping and petrography showed that the Inverian assemblage is also amphibolite-facies, whilst the earlier Badcallian is granulite-facies. Corfu et al. (1994) obtained U-Pb zircon ages of ~2710Ma and ~2490Ma which they attributed to the Badcallian and Inverian respectively, although Friend and Kinny (1995) interpreted an age of ~2490Ma to date the Badcallian tectonothermal event. Corfu et al. (1994) and Kinny and Friend (1997) both attributed U-Pb titanite ages of ~1750Ma to the Laxfordian event.

Methodology

Twenty-one samples of TTG gneisses and three samples of metasediments were collected from localities around the village of Scourie (Fig. 1b). These samples were chosen as they recorded a range of different tectonothermal histories: some preserved early Badcallian or Inverian assemblages and structures while others were pervasively altered in the Laxfordian. Rather than just collecting the most undeformed rocks possible, as in most zircon geochronological studies, samples with varying degrees of deformation enabled investigation into whether zircon lattice distortion is more frequent in deformed rocks.

Thin sections and rock chips (~3mm thickness) were cut from samples so that there was a petrographic context for any distorted zircons which could allow speculation as to the cause of lattice distortion. These were polished to 0.25µm grade using progressively finer diamond paste and finally colloidal silica solution. For SIMS analysis, the thin sections were cut up and the relevant parts were mounted onto a one inch glass round with epoxy resin suitable for the ion microprobe sample holder. Zircons were also mechanically separated from the same samples to increase the zircon population size. A population of fifty-five in-situ zircons and forty-four grain-mounted zircons from the twenty-four samples were analysed for lattice distortion.

Backscattered electron (BSE) and cathodoluminescence (CL) imaging were carried out in a Philips XL30 SEM at the University of Liverpool. EBSD was conducted on a CamScan X500 crystal probe with a thermionic field emission gun, also at University of Liverpool. Analytical parameters broadly follow that of Mariani et al. (2009) and Bestmann et al. (2006). Lattice misorientation maps

displayed in this contribution are composites of band contrast (the pattern quality of the EBSD data) and texture component (a false-colour map of crystallographic orientation relative to a given point) created in the Tango module of CHANNEL 5 software. EBSD maps are interpreted qualitatively, and quantitatively using a Burgers Vector analysis, to elucidate possible dislocation types responsible for lattice distortion (Wheeler et al., 2009) – this is the first published use of this method on a mineral.

SIMS analysis of zircon was carried out at the NERC Ion Microprobe Facility, University of Edinburgh. Trace elements were measured using a Cameca ims-4f ion microprobe while U-Th-Pb isotopic measurements were made using a Cameca 1270 ion microprobe. Analytical and correction procedures follow those outlined by Kelly and Harley (2005a) and Kelly et al. (2008). Analytical reproducibility of U/Pb ratios during and between analytical periods was calibrated against the 91500 (Wiedenbeck et al., 1995), SL1 (Maas et al., 1992) and Plesovice (Slama et al., 2008) zircon standards. Plesovice was the primary standard and yielded a mean $^{206}\text{Pb}/^{238}\text{U}$ ratio of 0.05359 ± 0.00023 (MSWD = 2.4; 95% conf.; $340.5 \pm 4.8\text{Ma}$; $n = 62$). U-Pb age plots and calculations were made using the computer program Isoplot 4.11 (Ludwig, 2003). All $^{207}\text{Pb}/^{206}\text{Pb}$ ages are quoted at 2σ uncertainty. Analytical reproducibility of trace elements was calibrated against the 91500 and SL1 zircon standard and the NIST SRM-610 glass standard (Hinton, 1999). For most REEs (middle-heavy), the average analytical error was $<10\%$ (2σ) but for some for the lighter REEs which have lower concentrations (La, Pr, Nd, Sm), it was higher. Analytical reproducibility against the NIST SRM610 glass standard was $<7\%$ (2σ) for all trace elements analysed.

Results

Distorted Zircons

EBSD analysis showed that five zircons out of the population of ninety-nine have internal lattice distortions of at least 3° . The five distorted zircons are described below in the context of their host rocks; three of these were analysed by ion microprobe for U-Th-Pb, Ti and REEs (Tables 1 & 2) and compared against undistorted zircons from the same population. Table 3 summarises the results

for each distorted zircon.

Zircon GG09/1 was located on a thin section from sample GG09, collected at UK Grid Reference NC 17947 41005, ~4.5km southeast of Scourie village (Geisgeil, Fig. 1b). At this locality, weakly-banded amphibolite-facies tonalitic gneiss is cut by a Scourie Dyke, which is in turn cut by a Laxfordian shear zone (Fig. 2a). Sample GG09 is from the pre-dyke banded tonalitic gneiss and is composed of ~40% hornblende aggregates, ~30% plagioclase, ~30% quartz and accessory biotite and opaques; there are no mineral shape fabrics in this rock (Fig. 3). It is interpreted to be a Badcallian granulite-facies gneiss that was subsequently pervasively statically retrogressed. Zircon GG09/1 (Fig. 4a) is a large and unusually squarish-shaped crystal, approximately 200x200µm in size; the lattice distortion is confined to one corner of the crystal, where the lattice gradually bends through 5° out to the tip. The CL pattern for this zircon is irregular – a narrow bright rim partially surrounds a CL-dark zone and fairly uniform lighter zone, which appears to have partially overprinted some earlier oscillatory zoning (Fig. 4a). Zircon GG09/1 was the only zircon found at this locality and so in the absence of undistorted zircons to compare it to, it was not analysed by ion microprobe.

Zircon ST02/2 was located on a thin section from sample ST02, collected at UK Grid Reference NC 14970 46124, ~1.5km northwest of Scourie village (Sithean Mor, Fig. 1b). At this locality, an enclave of metasemipelite is surrounded by tonalitic gneiss; the field relationships suggest the fabric in the metasemipelite may be pre-dyke as the fabric in the surrounding TTG gneiss is cross-cut by a Scourie dyke (Fig. 2b). Sample ST02 is from the metasemipelite and is composed of ~30% plagioclase, ~30% quartz aggregates, ~30% biotite laths and relict garnet porphyroblasts. There is a coarse mineral layering and the quartz aggregates define a shape fabric; biotite laths are not aligned and the garnet porphyroblasts are heavily fractured and retrogressed to biotite around the rims (Fig. 3). Zircon ST02/2 (Fig. 4b) is roughly elliptical and approximately 100µm in length along its long axis; there is lattice misorientation across the crystal of around 3° (Fig. 4b). BSE imaging reveals a brittle fracture, which correlates to a certain degree with the microstructure shown in the

EBSD map but there is still apparent lattice distortion on either side of this (Fig. 4b). The zircon is largely CL-dark with irregular patches of lighter CL response (Fig. 4b).

Zircon BP06/3 was located on a thin section from sample BP06, collected at UK Grid Reference NC 14565 41561, ~3.5km south-southeast of Scourie village (Badcall Point, Fig. 1b). At this locality, an early Badcallian gneissic layering in tonalitic gneiss is cut by a narrow band of possibly Inverian fabric; this is cut by a Laxfordian shear zone, which also cuts a Scourie Dyke (Fig. 2c). Sample BP06 is from the Laxfordian shear zone and is composed of ~75% sericitised plagioclase, ~20% hornblende and ~5% quartz with accessory allanite, titanite, ilmenite and rutile. Sub-millimetre hornblende crystals aggregate to define a moderate mineral aggregate lineation (Fig. 3). Zircon BP06/3 (Fig. 4c) is a large irregularly-shaped zircon, approximately 300x150µm in size; lattice distortion occurs in one half of this elongate crystal, up to 10° from the centre to the tip. The stepped nature of the misorientation profile indicates that this crystal is split into subgrains. BSE imaging shows a small fracture along one edge of the crystal, which is also picked up by EBSD but is unrelated to the lattice distortion shown by the EBSD (Fig. 4c).

The CL pattern is irregular – it is generally CL-dark with a slightly brighter rim (Fig. 4c). A brighter linear feature (a fracture) passes through the crystal but appears unrelated to the lattice distortion. There are many sinuous CL-dark lines sub-parallel to the subgrain walls shown by EBSD although they do not appear to correlate with the position of the subgrain walls; these sinuous CL-dark lines are similar to features noted by Reddy et al. (2006) and Timms et al. (2011), which they interpret to be subgrain walls.

Five ion microprobe analytical spots were made on this zircon (see Fig. 4c), two of which (4 & 5) were placed on subgrain walls with the other three in different microstructural domains of the crystal; the spot locations were checked after ion microprobe analysis with CL imaging. For the five spots, Th/U ratios range from 1.8-3.2 (Fig. 5a) while the $^{207}\text{Pb}/^{206}\text{Pb}$ ages fall between $2422\pm 20\text{Ma}$ and $2453\pm 16\text{Ma}$ (Fig. 5b). The five ages are well within error of each other, with discordance of -3.02% to +0.26%. Ti concentrations are between 5.7 and 10.7ppm (Fig. 6). Four of the five spots

show typical zircon REE patterns (Fig. 7a); zircons are enriched in heavy REEs relative to light REEs but also have a positive Ce anomaly and a negative Eu anomaly (Kelly and Harley, 2005a; Kelly and Harley, 2005b). However, spot 3 is depleted in heavy REEs with a Lu abundance of only 383ppm; this illustrated by the low Yb/Gd ratio of 7 relative to ≥ 10 for most undistorted zircons (Fig. 7b, Table 2). Numerous other zircons were found in this sample, including some located within a few millimetres of zircon BP06ChZ3, but all were undistorted.

Zircons DP02/2 and DP02/7 were located on a thin section from sample DP02, collected at UK Grid Reference NC 17923 35972, ~6km west-northwest of Kylesku village (Duartmore Point, Fig. 1b). At this locality, a Scourie Dyke cuts across Badcallian granulite-facies tonalitic gneisses but is rotated and sheared by a Laxfordian shear zone (Fig. 2d). Sample DP02 is from the Laxfordian shear zone and is composed of ~60% hornblende aggregates, ~35% sericitised plagioclase and ~5% quartz with accessory rutile, titanite, ilmenite and apatite. Sub-millimetre hornblende crystals aggregate to define strong mineral lineation (Fig. 3). Only two zircons were found in this sample big enough for ion microprobe analysis, and both show lattice distortion.

Zircon DP02/2 (Fig. 4d) is a small elliptical zircon, approximately 80 μ m in length along its long axis; there is up to 7° misorientation in a band running diagonally across the crystal with one fairly sharp boundary suggesting a fracture; BSE imaging does not clearly suggest this as a fracture. Due to the small size of the zircon, it was difficult to get a high-resolution CL image but it shows many sinuous dark lines, as in zircon BP06/3; some of these correlate with lines of dark blebs shown by BSE imaging, and with the lattice distortion pattern and therefore may represent subgrain walls. There is also a bright spot in the centre of the grain, which does not correspond with the microstructure (Fig. 4d). Just one ion microprobe analysis was made for this zircon due to its small size. The Th/U ratio is 0.49 (Fig. 5a) while the apparent $^{207}\text{Pb}/^{206}\text{Pb}$ age of $2331 \pm 22\text{Ma}$ is discordant by 6.3%, plotting well below concordia (Fig. 5b). Ti abundance is 22ppm (Fig. 6). Light REEs form a typical zircon pattern but there is no Eu anomaly (concentration of Eu is higher than Sm). The heavy REEs show a flatter profile relative to undistorted zircons (Fig. 7a), illustrated by a very low Yb/Gd

ratio of 4 (Fig. 7b); the concentration of Lu is only 137ppm.

Zircon DP02/7 (Fig. 4e) is a squat, slightly elliptical crystal, approximately 100x80µm in size; there is up to 15° variation in lattice orientation across the crystal, with the most extreme deformation occurring in opposite corners. The EBSD analysis also demonstrates an unusual cross-hatched pattern in lattice orientation in one part of the crystal, with misorientation of up to 7° here (Fig. 4e). BSE imaging shows the core of the grain to have some concentric zoning with fractures emanating from this (Fig. 4e). CL imaging shows the core to be very CL-dark which suggests high U content; the rim, including area of cross-hatched lattice distortion, is CL-bright (Fig. 4e). High U concentrations can induce metamictisation, which causes volume increase resulting in the radial fracture pattern (Corfu et al., 2003). While the rim has clearly formed before the metamictisation, it is difficult to say whether the cross-hatched lattice distortion occurred before the metamictisation or is related to it. Just one ion microprobe analysis was made for this zircon due to its small size; the spot was placed in an unfractured part of the CL-bright rim showing cross-hatched lattice distortion. The Th/U ratio is 0.28 (Fig. 5a) while the $^{207}\text{Pb}/^{206}\text{Pb}$ age of $2266\pm 40\text{Ma}$ is discordant by 8.5%, plotting well below concordia (Fig. 5b). Ti concentration is 47ppm (Fig. 6). The REE pattern is typical of that expected for zircon (Kelly and Harley, 2005a) (Fig. 7a).

Undistorted Zircons

Ion microprobe U-Th-Pb, Ti and REE data from three of the five distorted zircons were compared to undistorted zircons to illustrate the effects of lattice distortion on trace element mobility and isotope systematics, and the geological conclusions drawn from them. The samples to which the distorted zircons were compared, and the reasons why, are given in Table 4. EBSD analysis shows little or no lattice misorientation in undistorted zircons while brittle fractures are visible in BSE images (Fig. 8). Undistorted zircons from sample BP06 displayed a range of CL patterns comprising dark cores, oscillatory zoning patterns, bright overgrowths and various other patterns. Th/U ratios ranged from 0.6-2.2 (Fig. 5a) while apparent $^{207}\text{Pb}/^{206}\text{Pb}$ ages ranged from $2485\pm 30\text{Ma}$ to

2973±24Ma (Fig. 5b); discordance ranged from -2% to +11% (Table 1). Ti concentrations were 14-24ppm (Fig. 6). The REE patterns are typical of that expected for zircon but Yb/Gd ratios are lower than those recorded by Kelly and Harley (2005a) (Fig. 7b).

Only two zircons were located and analysed from sample DP02 and these both had distorted lattices. In order to investigate the effects of lattice distortion on their trace elements and isotopes, undistorted zircons from sample DP01 were used for comparison. This sample was located ~1m away from DP02 in the marginal part of the shear zone. Sample DP01 is composed of ~40% quartz, ~40% plagioclase and ~20% sieve-textured hornblende and quartz, after pyroxene, with accessory rutile, allanite, magnetite and apatite. There is no lineation, only weak gneissic layering and the sample is therefore much less intensely deformed than sample DP02. Undistorted zircons from sample DP01 displayed a range of CL patterns comprising dark cores, oscillatory zoning patterns, bright overgrowths and various other patterns. Th/U ratios ranged from 0.1-1.5 (Fig. 5a) while apparent $^{207}\text{Pb}/^{206}\text{Pb}$ ages ranged from 2430±44Ma to 3017±56Ma (Fig. 5b); discordance ranged from -6% to +7% (Table 1). Ti concentrations were 8-21ppm (Fig. 6). The REE patterns are typical of that expected for zircon but Yb/Gd ratios are lower than those recorded by Kelly and Harley (2005a) (Fig. 7b).

Discussion

Origin of the Lattice Distortion

It is outside the scope of this contribution to give a detailed description of the origin of distortion but it is relevant particularly in regard to the time at which distortion originated. Crystals with lattice distortion may have grown with defects (Penn and Banfield, 1998) and therefore have had a distorted lattice from the time of their initial formation; alternatively, post-crystallisation plastic deformation may occur through movement of lattice dislocations: if some of these remain in the lattice then it may be distorted. Little is known about zircon deformation so the general appearance of microstructures in other minerals is drawn upon to aid interpretation of the

microstructure in the distorted zircons in this study. A new method of analysing lattice distortion is applied, which gives some information on the Burgers vectors of the geometrically necessary dislocations responsible for distortion (Wheeler et al., 2009). In brief, the “integration” version of this method gives the *net* Burgers vector of all the dislocations passing through any chosen area on an EBSD map. These dislocations may be uniformly distributed, non-uniformly distributed or form subgrain walls.

The Weighted Burgers Vector (WBV) is expressed crystallographically, and is best presented normalised to the area of the loop (Fig. 9 and Table 5), so it is measured in $(\mu\text{m})^{-2}$ or 10^{12} m^{-2} (the former unit is more convenient). An example of the meaning of the WBV in Table 5 is as follows. A loop of square outline $10 \mu\text{m} \times 5 \mu\text{m}$, with a WBV of $(1, 0, 4) (\mu\text{m})^{-2}$, could mean that there are 50 dislocation lines with Burgers vector $[100]$ and 200 lines with Burgers vector $[001]$ passing through the square. Alternatively, it could mean that there are 50 dislocation lines with Burgers vector $[104]$. The WBV is an average over the areas of the loop and the types of dislocation threading through that loop – it proves useful, in trigonal, tetragonal and hexagonal phases, for distinguishing Burgers vectors lying in the basal plane from others. The Burgers vectors of dislocations are relevant for understanding the origins of distortion in all crystalline materials. For example, in quartz, Burgers vectors lie in the basal plane for low temperature deformation but can be parallel to the c axis for higher temperature deformation (e.g. Lister and Dornsiepen, 1982). The *relative* magnitudes of the (symmetrically equivalent) a and b components, and the c component which lies parallel to the 4-fold symmetry axis, are now discussed.

WBV data are overlaid on Texture Component EBSD maps for each of the distorted crystals (Fig. 9). Zircons GG09/1 and BP06/3 both have lattice distortion patterns suggestive of plastic deformation: the WBV shows variable directions probably due to a mix of dislocations with different Burgers vectors, and there are irregularly shaped subgrain walls. The irregular shapes are indistinguishable from subgrain wall morphologies seen in quartz (e.g. Gleason et al., 1993; Stipp and Tullis, 2003; Heilbronner and Tullis, 2006) and olivine (e.g. Drury, 2005). The distortion of one tip

of zircon GG09/1 suggests that that particular part of the crystal has been bent, showing that strain uptake in the zircon lattice was heterogeneous in its distribution. In zircon BP06/3, the subgrain structure with parallel subgrain walls also indicates bending of the lattice in a similar fashion. Zircon ST02/2 may also have had its lattice bent by plastic deformation. In zircon DP02/2, there is a crude radial pattern of subgrain walls around a slightly misoriented part. This could be a deformation microstructure influenced by the strength heterogeneity caused by the misoriented part, or it is conceivably caused by growth defects. The cross-hatched misorientation pattern in zircon DP02/7 is most unusual, with straight parallel subgrain walls. Boyle et al., (1998) found similar “checkerboard” microstructures in pyrite which were interpreted as being formed by slip parallel to the [100] planes. This suggests that the microstructure in zircon DP02/7 *might* be a deformation microstructure but it is yet more regular than the pyrite example. In addition to this, the WBV measurements are dominated by components lying in the *a* and *b* plane (the basal plane), suggesting that the cross-hatched misorientation pattern in zircon DP02/7 is a growth microstructure.

Trace Element Behaviour in Relation to Lattice Distortion

Before we discuss our interpretation, we outline two distinct ways in which a distorted lattice may influence chemistry. First, defects form fast diffusion pathways (Hart, 1957). Planar and linear defects can provide connections to the grain boundary network and hence provide pathways for chemical exchange between crystal and surroundings, as proposed for zircon by Reddy et al. (2006). Some lattice diffusion must be involved too, to move trace elements into or out from the defects, but over length scales much smaller than the grain size – and hence faster. Reddy et al. (2006), Timms et al. (2006b) and Timms et al. (2011) proposed that, in general, lattice distortion allowed enhanced ion movement along fast pathways such as subgrain walls; this generally led to depletion of trace elements in the zircon.

Secondly, dislocations and subgrain walls are defects and an *equilibrium* partitioning of trace elements between defects and pristine lattice is to be expected. For example, impurity atoms may

have a higher equilibrium concentration near a dislocation (Cottrell and Bilby, 1949) – since referred to as a “Cottrell atmosphere” (e.g. Takeuchi and Argon, 1979; Wilde et al., 2000; Zhao et al., 2001). This is because the defect has a local stress field which modifies the chemical potentials of impurities (e.g. Larche and Cahn, 1985). A similar effect is to be expected in a subgrain wall since it is an arrangement of dislocations, as well as at interfaces because although they generally have no long range stress field, they have a relatively disordered structure and hence can incorporate higher concentrations of trace elements (e.g. Hiraga et al., 2003; Pinilla et al., 2012). This was found to occur in olivine by Ando et al. (2001): Fe partitions preferentially into subgrain walls. Equilibrium concentrations will vary only very close to the defects: for example the stress field of a dislocation dies away over a length scale of the order of the Burgers vector. However, the introduction of a subgrain wall into a lattice would likely cause trace elements to diffuse from the pristine lattice into the wall, thus creating larger scale chemical variations if diffusion gradients are frozen in. This would lower the concentration in the lattice but keep the average concentration fixed.

These two separate effects of distorted lattice on chemistry, which are not mutually exclusive, must form the foundation for our discussion. Generally, when we note a correlation between lattice distortion and trace element concentrations from spots including distorted lattice, we favour the first explanation (fast diffusion pathways). This is because a “repartitioning” of trace elements between lattice and subgrain walls as a result of distortion would not change the *average* concentration over a spot which encompassed several walls. In contrast, establishing a fast connection to the grain surroundings would facilitate a variety of changes in concentration, depending on the surrounding chemistry.

As “repartitioning” would not change the *average* concentration over an ion microprobe analytical spot, the same would apply for a whole-grain TIMS analysis. While we focus on effects of lattice distortion on trace elements measured by ion microprobe in this study, TIMS is also widely used in zircon geochronology and so it is instructive to discuss the potential whole-grain effects of lattice distortion. Subgrain walls acting as fast diffusion pathways appear to be the key facilitator of

chemical alteration and so the volume of zircon in which these are present would be expected to be roughly proportional to the degree of chemical disturbance. For example, a high resolution ion microprobe spot which sampled subgrain wall would be expected to have a different chemical signature to a spot which sampled pristine lattice in another part of the same grain. A whole grain TIMS analysis, however, would record a chemical signature somewhere between that of the two ion microprobe spots. While a detailed study of this is beyond the scope of this study, it may be worth consideration in TIMS geochronological studies.

Comparison of Distorted and Undistorted Zircons

U-Th-Pb

As U-Pb zircon dating is a widely used technique, it is important to understand the effects of lattice distortion on U-Th-Pb systematics. Th/U ratios of 1.8-3.2 in zircon BP06/3 were generally higher than those of the undistorted comparison zircons from the same sample (generally in the range of 0.6-2.2) (Fig. 5a). The bulk U and Th contents in this zircon were among the highest in the whole population but this is not interpreted to be related to lattice distortion – an undistorted zircon located ~8mm away also has high Th and U and this is interpreted to be a due to local Th and U availability during growth or metamorphic recrystallization. Zircons DP02/2 and DP02/7 had Th/U ratios of 0.49 and 0.28, respectively, which fall within the range of the comparison zircons from sample DP01 (0.15-1.54) but are lower than the average of 0.6 (Fig. 5a).

Seven of the eight youngest apparent $^{207}\text{Pb}/^{206}\text{Pb}$ ages in the population ($n = 45$) are from distorted zircons (Fig. 5b). The five ages from zircon BP06/3 are discordant by +0.5% to -3%. Timms et al., (2006b) noted that reverse discordance may be explained by U loss through open-system behaviour during bending of the lattice. In this study, however, the discordance is within error of concordia at 2σ confidence levels and may therefore be an analytical artefact. The five ages from this zircon are younger than, and not within 2σ error of, previously published ages of 2490Ma for a tectonothermal event in the Central Region/Assynt Terrane (Corfu et al., 1994; Friend and Kinny,

1995). A small amount of Pb-loss from the lattice during lattice distortion would give an age slightly younger than crystallisation, suggesting plastic deformation occurred at ~2490Ma. This distorted zircon was sampled from within a few metres of a member of the Scourie Dyke Swarm which intruded at ~2000-2400Ma (Heaman and Tarney, 1989). It is possible that an increase in temperature caused by the nearby intrusion of the hot dyke material caused the small amount of Pb lost, shifting the analytical data-points a short distance down the concordia curve. As this is not recorded in undistorted zircons, the temperature increase may have been just enough to cause diffusion of Pb in distorted zircon lattice but not undistorted zircon lattice.

Zircons DP02/2 and DP02/7 give ages that are younger than all the other analysed zircons in this study, with or without lattice distortion. They are relatively discordant (+6.28% and +8.49%, respectively) and plot below concordia (Fig. 5b). CL images of these two zircons (Fig. 4) do not show any overgrowths younger than ~2400Ma which the ion microprobe spots could have sampled, resulting in a mixed age. Their discordant position on the concordia plot (Fig. 5b) is therefore interpreted to be due to Pb-loss. The position and spatial relationship of the ellipses for DP02/2 and DP02/7 on a concordia plot line up on a discordia chord with an upper intercept through a cluster of concordant (+5% to -1%) ages of ~2500Ma from undistorted zircons from samples DP01 and BP06 (Fig. 5c). This discordia has an upper intercept at 2571 ± 51 Ma and a lower intercept at 1631 ± 250 Ma with a MSWD of 2.5 at 2σ confidence levels (Fig. 5c). The age cluster at ~2500Ma is interpreted to be the age of a tectonothermal event – it is the youngest concordant zircon age recorded in the whole dataset and is also close to the 2490Ma tectonothermal event (the Inverian of Corfu et al. (1994) and the Badcallian of Kinny et al. (2005)). Although the lower intercept has a large error, it is within error of published ages for the lower amphibolite-facies Laxfordian tectonothermal event. Kinny and Friend (1997) and Corfu et al. (1994) give $^{207}\text{Pb}/^{206}\text{Pb}$ ages of 1750-1670Ma from rutile and titanite for the Laxfordian. Therefore, these two zircons could potentially be recording the Laxfordian event in their U-Pb systematics. An increase in temperature in the Laxfordian may have allowed diffusion of Pb out of the zircon aided by the inherent lattice distortions. Laxfordian ages are not recorded in

any undistorted zircons in this study or in previous studies which suggests that lattice distortion allows Pb diffusion at lower temperatures than in undistorted zircon, effectively locally lowering the closure temperature.

Ti Thermometry

Ti content in zircon increases with equilibration temperature in the presence of rutile– this forms the basis of the Ti-in-zircon geothermometer derived by Watson et al., (2006). The accuracy of the temperatures calculated with the Ti-in-zircon thermometer is controlled by a_{TiO_2} – excess rutile in the rock indicates that the $a_{\text{TiO}_2} = 1$ and Ti content in zircon was buffered. In this case, the calculated temperatures will be accurate. If there is no rutile present during zircon crystallisation, the system is not buffered and the calculated temperature will be a minimum. Quartz and accessory rutile is present in samples BP06, DP02 and DP01 so all zircon temperatures calculated in this study are interpreted to be accurate.

Using the updated thermometer calibration of Ferry and Watson (2007), zircon BP06/3 records temperatures of $696 \pm 19^\circ\text{C}$ to $752 \pm 24^\circ\text{C}$. Undistorted zircons from this sample record higher temperatures, ranging from $783 \pm 27^\circ\text{C}$ to $834 \pm 33^\circ\text{C}$ (Table 2), including one zircon located approximately 2mm away from distorted zircon BP06/3 which recorded a temperature of $791 \pm 28^\circ\text{C}$. This indicates that the distorted zircon has lost Ti from its lattice, most likely as a result of lattice distortion. Zircon DP02/2 yields a crystallisation temperature of $820 \pm 32^\circ\text{C}$ which is at the upper end of the range of $729 \pm 22^\circ\text{C}$ to $819 \pm 32^\circ\text{C}$ recorded in undistorted zircons from sample DP01. Lattice distortion is interpreted not to have had any extreme or obvious effects on this particular crystal. In zircon DP02/7, however, the temperature recorded is $914 \pm 44^\circ\text{C}$, 94° higher than any of the other zircons in the population. The high temperature recorded by zircon DP02/7 could reflect local Ti buffering with the other zircons only recording minimum temperatures. However, zircon DP02/2, located ~8mm from DP02/7, records a temperature 94° lower; this hypothesis would therefore require a considerable variation in Ti availability over that short distance which seems unlikely.

Furthermore, accessory rutile is present in samples DP01 and DP02 so the thermometer temperatures are interpreted to be accurate.

A more likely explanation is that Ti has partitioned preferentially into the distorted zircon lattice forming a Cottrell atmosphere as described above. The Ti-in-zircon geothermometer is based on Ti concentration in pristine lattice. For a given temperature, Ti concentration in a Cottrell atmosphere will be higher than in pristine lattice and a falsely high temperature will be calculated if the distortion is not considered. It should also be noted that zircon DP02/7 has many fractures. Care was taken to place the ion microprobe spot on part of the zircon rim which was not fractured but it is possible that the analysis may have sampled a fracture beneath the polished surface. Harrison and Schmidt (2007) showed that Ti was concentrated in fractures and this is another possible explanation for the high Ti content in this zircon. In summary the Ti abundances in our distorted zircons (and the zircon megacryst investigated by Timms et al. (2011)) are best explained in terms of distorted lattices being fast diffusion pathways *and* zones into which Ti partitions preferentially.

Zircon DP02/7 appears to have been most extremely affected by lattice distortion but the degree of misorientation on the subgrain walls is less than that in zircon BP06/3 where the temperature has been affected by lattice distortion to a lesser degree. This suggests that there is no correlation between the degree of misorientation and the magnitude of chemical disturbance.

REEs

The zircons with no lattice distortion from samples BP06 and DP01 show a typical chondrite-normalised zircon REE pattern of increasing abundance from light to heavy REE, with positive Ce anomaly and negative Eu anomaly (Kelly and Harley, 2005a). However, Yb/Gd ratios (Fig. 7b) were generally lower than those recorded by Kelly and Harley (2005a) and there was more than an order of magnitude of variation in the chondrite-normalised concentration of the heaviest REEs (Fig. 7a). The REE profiles of undistorted zircons from samples BP06 and DP01 were similar and therefore pooled for comparison against the zircons with lattice distortion.

Distorted zircon BP06/3 generally follows the normal pattern but with some deviation and heterogeneity within the crystal: spot 3 has a relatively low concentration of heavy REEs and a slightly flatter heavy REE profile ($\text{Yb/Gd} = 7$); and the Eu anomaly is subdued, with spot 5 actually having more Eu than Sm, the previous element. The Sm/Nd ratio is low – 1.5-2.5 relative to generally 3-6 in undistorted zircons (Fig. 7c). Spot 1, with the highest chondrite-normalised REE abundance, falls on the least distorted lattice (Fig. 4c and Table 5), whilst spots 3-5 clearly intersect at least one subgrain wall, have higher WBV values, and have lower REE abundances. There is not a simple correlation between WBV values and REE concentration, however.

The REE abundances of distorted zircon DP02/7 fall within the range of undistorted zircons but with a subdued Eu anomaly – the negative Eu anomaly is not as pronounced as in undistorted zircons (Fig. 7a). Zircon DP02/2 also has a subdued Eu anomaly, with more Eu than Sm. It also has a relatively flat heavy REE pattern, illustrated by a low Yb/Gd ratio of 4. Analyses from both DP02/2 and DP02/7 were from spots which include many subgrain walls (Fig. 4d&e).

On the whole, REE profiles from distorted zircons are within the range of those from undistorted zircons. DP02/2 and one analysis from BP06/3 have low Yb/Gd ratios but a small number of analyses from undistorted zircons also have low Yb/Gd values so the relative depletion in heavy REEs cannot be confidently ascribed to enhanced diffusion due to lattice distortion. Taken together, distorted zircon DP02/2, DP02/7 and BP06/3 show a tentative correlation between distortion and lower REE concentrations, particularly heavy REEs. This cannot be explained by “Cottrell atmospheres” of REEs because we expect *higher* concentrations around defects. Cherniak et al. (1997) showed that heavy REEs diffuse faster than lighter REEs in an undistorted zircon lattice. Diffusion rates would increase with the fast volume diffusion pathways created by lattice distortion and result in the flattening of the middle-heavy REE pattern. A change in partition coefficients between zircons and other phases due to changing pressure-temperature conditions a possible driver for diffusion – the different patterns from DP02/2 and DP02/7 may be influenced by spot size relative to grain size and defect density. Fluids circulating through the rock may also have been a

driver for heavy REE loss. Pal et al. (2011) showed that heavy REEs are more strongly complexed with fluorine-rich fluids than light REEs.

Implications of Lattice Distortion

Three of the five distorted zircons were found in samples from Laxfordian shear zones. These are strongly deformed rocks and it would be reasonable to infer that there is a link between deformation at the whole-rock scale and lattice distortion of the zircons. However, WBV analysis suggests that the lattice distortion in zircons DP02/2 and DP02/7 was not caused by plastic deformation and is therefore unrelated to the shear zone deformation. Zircon BP06/3 is also from a Laxfordian shear zone and does appear to have been distorted by plastic deformation. However, whether the plastic deformation is directly related to the shearing is not clear as nine undeformed zircons were found in the same sample. In samples from shear zones as a whole, a total of three distorted zircons and twenty-five undistorted zircons were found. One (ST02/2) of fifteen zircon from metasemipelite samples has a distorted lattice while one (GG09/1) of fifty-five zircons from non-shear zone TTG gneiss samples has a distorted lattice. That only a small number of zircons were distorted, even in shear zone rocks, and that they were located in close proximity to undistorted zircons, indicates there is no clear link between macro-scale deformation and intracrystal zircon distortion. From this study, it would appear that although lattice distortion has an effect on zircon trace element abundances and isotope systematics, the frequency of lattice distortion in a population of zircons is low. It is unlikely to have a major impact on a typical zircon geochronology study, especially where the least deformed rocks are sampled. Furthermore, given a large population size, anomalous data yielded by zircons with lattice distortion would be discarded regardless of whether it is known that the zircons are distorted or not. However, when investigating zircon from shear zone rocks, for example to date deformation events, there may be a case for EBSD analysis.

Conclusions

Analysis of a range of trace elements and isotopes in a population of zircons from variably deformed and metamorphosed rocks of the Lewisian Gneiss Complex of northwest Scotland has raised the following key points:

1. Five of ninety-nine zircons analysed were found to have distorted lattices. Three of these were from shear zone rocks while one was from a non-shear zone TTG gneiss and the other from a metasemipelite.
2. Weighted Burgers Vectors analysis suggests that three of the five distorted zircons have undergone post-crystallisation plastic deformation to distort their crystal lattices; the other two have lattice distortion patterns not easily explained by plastic deformation and are instead interpreted to have grown with distorted lattices.
3. Zircon trace element abundances and isotope systematics appear to have been affected by lattice distortion where it has occurred. Zircon BP06/3 has high Th/U ratios and slightly young ages reflecting minor Pb loss, relative to zircons from the same sample with no lattice distortion. There is some intracrystal heterogeneity in Ti content and it is generally relatively low, yielding five of the youngest seven Ti-in-zircon thermometer temperatures. Rare earth element (REE) profiles are generally within the range of undistorted zircons although one analytical spot had a relatively low Yb/Gd ratio. Zircons DP02/2 and DP02/7 differ from BP06/3 in that Th/U ratios are low and Pb-loss significant. There are differences between zircons DP02Z2 and DP02Z7, however: DP02Z7 has a significantly higher Ti content while DP02Z2 has a relatively low Yb/Gd ratio.
4. Differences in trace element abundances and isotope systematics in distorted zircons relative to undistorted zircons are interpreted to have been facilitated by subgrain walls – a key feature of lattice distortion in zircon. Trace elements and isotopes would have moved from undistorted lattice into these subgrain walls as their chemical potential is modified due to the presence of the dislocations which make up the subgrain wall. Subgrain walls provided pathways for chemical exchange between crystal and surroundings.

5. Discordant apparent $^{207}\text{Pb}/^{206}\text{Pb}$ ages of $2331\pm 22\text{Ma}$ and $2266\pm 40\text{Ma}$ from two distorted zircons define a discordia lower intercept within error of the previously recorded age of the lower-amphibolite-facies Laxfordian tectonothermal event. Undistorted zircons do not record Laxfordian ages. This suggests that lattice distortion allows Pb diffusion at lower temperatures than in undistorted zircon. Distorted zircons may therefore record information about lower temperature geological events not otherwise recorded in undistorted zircons.

Overall, these findings illustrate the variable effects of crystal lattice distortion on trace element mobility and isotope systematics in zircon. The low frequency of lattice distortion, however, suggests that lattice distortion would not have a major impact on zircon populations analysed in typical geochronology studies. There may be a case for conducting EBSD analysis prior to ion microprobe analysis if the zircons are sourced from highly deformed rocks as the majority of distorted zircons in this study were found in shear zone rocks.

Acknowledgements

This work was carried out under UK Natural Environment Research Council DTG NE/G523855/1 and British Geological Survey CASE Studentship 2K08E010 to JMM. Carmel Pinnington and Eddie Dempsey are thanked for assistance with SEM analysis. Ion microprobe analysis at the Edinburgh Ion Microprobe Facility was carried out with funding from NERC grant IMF384/1109; Richard Hinton, Cees-Jan De Hoog and John Craven are thanked for ion microprobe support and Mike Hall for assistance with sample preparation. Detailed reviews by Martin Whitehouse and an anonymous reviewer, plus discussions with Alan Boyle, Craig Storey and Nick Roberts, considerably improved this manuscript. KMG publishes with the permission of the Executive Director of the Geological Survey.

Figure Captions

Fig. 1 Location maps: a: Outline map of NW Scotland, shaded areas denote LGC outcrop and dotted box denotes location of map b; location within British Isles in inset; b: Map of Scourie area showing the location and geological context of the field localities.

Fig. 2 Maps of field areas from which analysed zircons were obtained; a: Geisgeil; b: Sithean Mor; c: Badcall Point; d: Duartmore Point; UK grid references given for each locality.

Fig. 3 Petrographic context of the distorted zircons: plane polarised light photomicrographs of each sample containing a distorted zircon; Hbl = hornblende, Plag = plagioclase, Qtz = quartz, Grt = garnet, Bt = biotite, Opq = opaque iron oxide.

Fig. 4 BSE images, CL images, lattice misorientation maps and misorientation profiles of the five zircons with lattice distortion. The lattice misorientation maps were generated using the “Texture Component” function in the “Tango” module of Channel5 software and illustrate crystallographic orientation relative to a given point. The misorientation profiles show this relative change along a transect. The location of the misorientation profiles are shown by the lines on the associated lattice misorientation maps. Ellipses denote ion microprobe analytical spot locations; on zircon BP06/3, numbers denote spot numbers referred to in the text. a: GG09/1; b: ST02/2; c: BP06/3; d: DP02/2; e: DP02/7.

Fig. 5 U-Th-Pb data: a Plot showing Th (ppm) against U (ppm) (with Th/U ratio contoured) of distorted and undistorted zircons; b Wetherill concordia plot showing the age relationship of distorted zircons BP06/3, DP02/2 and DP02/7 and undistorted comparison zircons from samples DP01 and BP06; c Concordia plot showing a discordia chord through the ellipses for DP02/2 and DP02/7 which has a lower intercept within error of the age of the Laxfordian tectonothermal event.

Fig. 6 Histogram showing the concentrations of Ti in distorted and undistorted zircons.

Fig. 7 Rare earth element (REE) data: a: Matsuda diagram showing REE profiles and concentrations; shaded area denotes analyses of undistorted comparison zircons, solid lines denote distorted zircons; values are normalised against chondrite (McDonough and Sun, 1995). b: Histogram of Yb/Gd ratios of distorted and undistorted zircons. c: Histogram of Sm/Nd ratios of distorted and undistorted zircons.

Fig. 8 BSE images, lattice misorientation maps and misorientation profiles of examples of zircons without lattice distortion (a) and zircons with fractures (b).

Fig. 9 Lattice distortion maps (as in Fig. 3) together with the WBV for some example rectangular subareas. The three numbers listed are the *a*, *b* and *c* components of the WBV, measured in $(\mu\text{m})^{-2}$.

Table Captions

Table 1 Ion microprobe U-Th-Pb data for distorted and undistorted zircons; analysis ID format is sample name/zircon number-spot number, so BP06/3-1 is spot 1 on zircon 3 from sample BP06.

Table 2 Ion microprobe trace element concentrations (parts per million); Ti Temp denotes crystallisation temperature calculated using the calibration of Ferry and Watson (2007) of the Ti-in-zircon thermometer (Watson et al., 2006).

Table 3 Summary table of microstructural and chemical characteristics of the five distorted zircons.

636 Table 4 Samples from which undistorted zircons have been used for comparison with distorted
1 637 zircons and the justification for sample choice.
2

3 638 Table 5 Weighted Burgers Vectors (WBV) data. For BP06 the areas correspond approximately to
4 639 some of the spots, as indicated.
5
6

7 640

8
9 641

10
11 642

12
13 643

14
15 644

16
17

18

19

20

21

22

23

24

25

26

27

28

29

30

31

32

33

34

35

36

37

38

39

40

41

42

43

44

45

46

47

48

49

50

51

52

53

54

55

56

57

58

59

60

61

62

63

64

65

References

- 1 Ando, J. et al., 2001. Striped iron zoning of olivine induced by dislocation creep in deformed
2 peridotites. *Nature*, 414(6866): 893-895.
- 3 Bestmann, M., Prior, D.J., Grasemann, B., 2006. Characterisation of deformation and flow mechanics
4 around porphyroclasts in a calcite marble ultramylonite by means of EBSD analysis.
5 *Tectonophysics*, 413(3-4): 185-200.
- 6 Boyle, A.P., Prior, D.J., Banham, M.H., Timms, N.E., 1998. Plastic deformation of metamorphic pyrite:
7 new evidence from electron-backscatter diffraction and foreshadow orientation-contrast
8 imaging. *Mineralium Deposita*, 34(1): 71-81.
- 9 Cherniak, D.J., Hanchar, J.M., Watson, E.B., 1997. Rare-earth diffusion in zircon. *Chemical Geology*,
10 134(4): 289-301.
- 11 Cherniak, D.J., Watson, E.B., 2003. Diffusion in Zircon. In: Hanchar, J.M., Hoskin, P.W.O. (Eds.),
12 Zircon. *Reviews in Mineralogy and Geochemistry*. Mineralogical Society of America and The
13 Geochemical Society.
- 14 Corfu, F., Hanchar, J.M., Hoskin, P.W.O., Kinny, P.D., 2003. Atlas of Zircon Textures. In: Hanchar, J.M.,
15 Hoskin, P.W.O. (Eds.), Zircon. *Reviews in Mineralogy and Geochemistry*. Mineralogical
16 Society of America and The Geochemical Society.
- 17 Corfu, F., Heaman, L.M., Rogers, G., 1994. Polymetamorphic Evolution of the Lewisian Complex, NW
18 Scotland, as Recorded by U-Pb Isotopic Compositions of Zircon, Titanite and Rutile.
19 *Contributions to Mineralogy and Petrology*, 117(3): 215-228.
- 20 Cottrell, A.H., Bilby, B.A., 1949. Dislocation Theory of Yielding and Strain Ageing of Iron Proceedings
21 of the Physical Society Section A, 62(1): 49-62.
- 22 Drury, M.R., 2005. Dynamic recrystallization and strain softening of olivine aggregates in the
23 laboratory and the lithosphere. *Geological Society, London, Special Publications*, 243(1):
24 143-158.
- 25 Evans, C.R., 1965. Geochronology of the Lewisian Basement near Lochinver, Sutherland. *Nature*, 204:
26 638-641.
- 27 Ferry, J.M., Watson, E.B., 2007. New thermodynamic models and revised calibrations for the Ti-in-
28 zircon and Zr-in-rutile thermometers. *Contributions to Mineralogy and Petrology*, 154(4):
29 429-437.
- 30 Finch, R.J., Hanchar, J., 2003. Structure and Chemistry of Zircon and Zircon-group Minerals. In:
31 Hanchar, J., Hoskin, P.W.O. (Eds.), Zircon. *Reviews in Mineralogy and Geochemistry*.
32 Mineralogical Society of America and The Geochemical Society.
- 33 Friend, C.R.L., Kinny, P.D., 1995. New Evidence for Protolith Ages of Lewisian Granulites, Northwest
34 Scotland. *Geology*, 23(11): 1027-1030.
- 35 Gleason, G.C., Tullis, J., Heidelbach, F., 1993. The role of dynamic recrystallization in the
36 development of lattice preferred orientations in experimentally deformed quartz
37 aggregates. *Journal of Structural Geology*, 15(9-10): 1145-1168.
- 38 Harrison, T.M., Schmitt, A.K., 2007. High sensitivity mapping of Ti distributions in Hadean zircons.
39 *Earth and Planetary Science Letters*, 261(1-2): 9-19.
- 40 Hart, E.W., 1957. On the Role of Dislocations in Bulk Diffusion. *Acta Metallurgica*, 5(10): 597-597.
- 41 Heaman, L.M., Tarney, J., 1989. U-Pb Baddeleyite Ages for the Scourie Dyke Swarm, Scotland -
42 Evidence for 2 Distinct Intrusion Events. *Nature*, 340(6236): 705-708.
- 43 Heilbronner, R., Tullis, J., 2006. Evolution of c axis pole figures and grain size during dynamic
44 recrystallization: Results from experimentally sheared quartzite. *J. Geophys. Res.*, 111(B10):
45 B10202.
- 46 Hinton, R.W., 1999. NIST SRM 610, 611 and SRM 612, 613 multi-element glasses: Constraints from
47 element abundance ratios measured by microprobe techniques. *Geostandards Newsletter-
48 the Journal of Geostandards and Geoanalysis*, 23(2): 197-207.
- 49 Hiraga, T., Anderson, I.M., Kohlstedt, D.L., 2003. Chemistry of grain boundaries in mantle rocks.
50 *American Mineralogist*, 88(7): 1015-1019.

- 1 Kelly, N.M., Harley, S.L., 2005a. An integrated microtextural and chemical approach to zircon
2 geochronology: refining the Archaean history of the Napier Complex, east Antarctica.
3 *Contributions to Mineralogy and Petrology*, 149(1): 57-84.
- 4 Kelly, N.M., Harley, S.L., 2005b. Timing of zircon growth during highgrade metamorphism:
5 Constraints from garnet-zircon REE. *Geochimica Et Cosmochimica Acta*, 69(10): A22-A22.
- 6 Kelly, N.M., Hinton, R.W., Harley, S.L., Appleby, S.K., 2008. New SIMS U-Pb zircon ages from the
7 Langavat Belt, South Harris, NW Scotland: implications for the Lewisian terrane model.
8 *Journal of the Geological Society*, 165: 967-981.
- 9 Kinny, P.D., Friend, C.R.L., 1997. U-Pb isotopic evidence for the accretion of different crustal blocks
10 to form the Lewisian Complex of northwest Scotland. *Contributions to Mineralogy and*
11 *Petrology*, 129: 326-340.
- 12 Kinny, P.D., Friend, C.R.L., Love, G.J., 2005. Proposal for a terrane-based nomenclature for the
13 Lewisian Gneiss Complex of NW Scotland. *Journal of the Geological Society*, 162: 175-186.
- 14 Larche, F.C., Cahn, J.W., 1985. The Interactions of Composition and Stress in Crystalline Solids. *Acta*
15 *Metallurgica*, 33(3): 331-357.
- 16 Lister, G.S., Dornsiepen, U.F., 1982. Fabric Transitions in the Saxony Granulite Terrain. *Journal of*
17 *Structural Geology*, 4(1): 81-92.
- 18 Ludwig, K.R., 2003. User's manual for Isoplot 3.00: a geochronological toolkit for Excel. Special
19 Publications, 4. Berkeley Geochronological Center.
- 20 Maas, R., Kinny, P.D., Williams, I.S., Froude, D.O., Compston, W., 1992. The Earths Oldest Known
21 Crust - a Geochronological and Geochemical Study of 3900-4200 Ma Old Detrital Zircons
22 from Mt Narryer and Jack Hills, Western-Australia. *Geochimica Et Cosmochimica Acta*, 56(3):
23 1281-1300.
- 24 Mariani, E., Mecklenburgh, J., Wheeler, J., Prior, D.J., Heidelbach, F., 2009. Microstructure evolution
25 and recrystallization during creep of MgO single crystals. *Acta Materialia*, 57(6): 1886-1898.
- 26 McDonough, W.F., Sun, S.s., 1995. The composition of the Earth. *Chemical Geology*, 120(3-4): 223-
27 253.
- 28 Pal, D.C., Chaudhuri, T., McFarlane, C., Mukherjee, A., Sarangi, A.K., 2011. Mineral Chemistry and In
29 Situ Dating of Allanite, and Geochemistry of Its Host Rocks in the Bagjata Uranium Mine,
30 Singhbhum Shear Zone, India-Implications for the Chemical Evolution of REE Mineralization
31 and Mobilization. *Economic Geology*, 106(7): 1155-1171.
- 32 Park, R.G., 1970. Observations on Lewisian Chronology. *Scottish Journal of Geology*, 6(4): 379-399.
- 33 Peach, B.N., Horne, J., Gunn, W., Clough, C.T., Hinxman, L.W., 1907. The Geological Structure of the
34 Northwest Highlands of Scotland. *Memoirs of the Geological Survey*. H.M.S.O., London.
- 35 Penn, R.L., Banfield, J.F., 1998. Imperfect oriented attachment: Dislocation generation in defect-free
36 nanocrystals. *Science*, 281(5379): 969-971.
- 37 Piazzolo, S., Austrheim, H., Whitehouse, M., 2012. Brittle-ductile microfabrics in naturally deformed
38 zircon: Deformation mechanisms and consequences for U-Pb dating. *American Mineralogist*,
39 97(10): 1544-1563.
- 40 Pinilla, C., Davis, S.A., Scott, T.B., Allan, N.L., Blundy, J.D., 2012. Interfacial storage of noble gases and
41 other trace elements in magmatic systems. *Earth and Planetary Science Letters*, 319: 287-
42 294.
- 43 Prior, D.J. et al., 1999. The application of electron backscatter diffraction and orientation contrast
44 imaging in the SEM to textural problems in rocks. *American Mineralogist*, 84(11-12): 1741-
45 1759.
- 46 Prior, D.J., Mariani, E., Wheeler, J., 2009. EBSD in the Earth Sciences: applications, common practice
47 and challenges. In: Schwartz, A.J., Kumar, M., Adams, B.L., Field, D.P. (Eds.), *Electron*
48 *Backscatter Diffraction in Materials Science*. Springer.
- 49 Reddy, S.M. et al., 2006. Crystal-plastic deformation of zircon: A defect in the assumption of
50 chemical robustness. *Geology*, 34(4): 257-260.

- Slama, J. et al., 2008. Plesovice zircon - A new natural reference material for U-Pb and Hf isotopic microanalysis. *Chemical Geology*, 249(1-2): 1-35.
- Stipp, M., Tullis, J., 2003. The recrystallized grain size piezometer for quartz. *Geophysical Research Letters*, 30: 2088-2093.
- Sutton, J., Watson, J., 1951. The pre-Torridonian metamorphic history of the Loch Torridon and Scourie areas in the North-West Highlands, and its bearing on the chronological classification of the Lewisian. *Quarterly Journal of the Geological Society*, 106: 241-296.
- Takeuchi, S., Argon, A.S., 1979. Glide and Climb Resistance to the Motion of an Edge Dislocation Due to Dragging a Cottrell Atmosphere. *Philosophical Magazine a-Physics of Condensed Matter Structure Defects and Mechanical Properties*, 40(1): 65-75.
- Tarney, J., Weaver, B.L., 1987. Geochemistry of the Scourian Complex: petrogenesis and tectonic models. In: Park, R.G., Tarney, J. (Eds.), *Evolution of the Lewisian and Comparable Precambrian High-Grade Terrains*. Blackwells.
- Timms, N.E., Kinny, P.D., Reddy, S.M., 2006a. Deformation-related modification of U and Th in zircon. *Geochimica Et Cosmochimica Acta*, 70(18): A651-A651.
- Timms, N.E., Kinny, P.D., Reddy, S.M., 2006b. Enhanced diffusion of Uranium and Thorium linked to crystal plasticity in zircon. *Geochemical Transactions*, 7: 1-16.
- Timms, N.E. et al., 2011. Relationship among titanium, rare earth elements, U-Pb ages and deformation microstructures in zircon: Implications for Ti-in-zircon thermometry. *Chemical Geology*, 280(1-2): 33-46.
- Watson, E.B., Wark, D.A., Thomas, J.B., 2006. Crystallization thermometers for zircon and rutile. *Contributions to Mineralogy and Petrology*, 151(4): 413-433.
- Wheeler, J. et al., 2009. The weighted Burgers vector: a new quantity for constraining dislocation densities and types using electron backscatter diffraction on 2D sections through crystalline materials. *Journal of Microscopy*, 233(3): 482-494.
- Wiedenbeck, M. et al., 1995. Three natural zircon standards for U-Th-Pb, Lu-Hf, trace element and REE analyses. *Geostandards Newsletter*, 19(1): 1-23.
- Wilde, J., Cerezo, A., Smith, G.D.W., 2000. Three-dimensional atomic-scale mapping of a cottrell atmosphere around a dislocation in iron. *Scripta Materialia*, 43(1): 39-48.
- Zhao, J.Z., De, A.K., De Cooman, B.C., 2001. Formation of the Cottrell atmosphere during strain aging of bake-hardenable steels. *Metallurgical and Materials Transactions a-Physical Metallurgy and Materials Science*, 32(2): 417-423.

Figure
[Click here to download Figure: Fig. 1.eps](#)

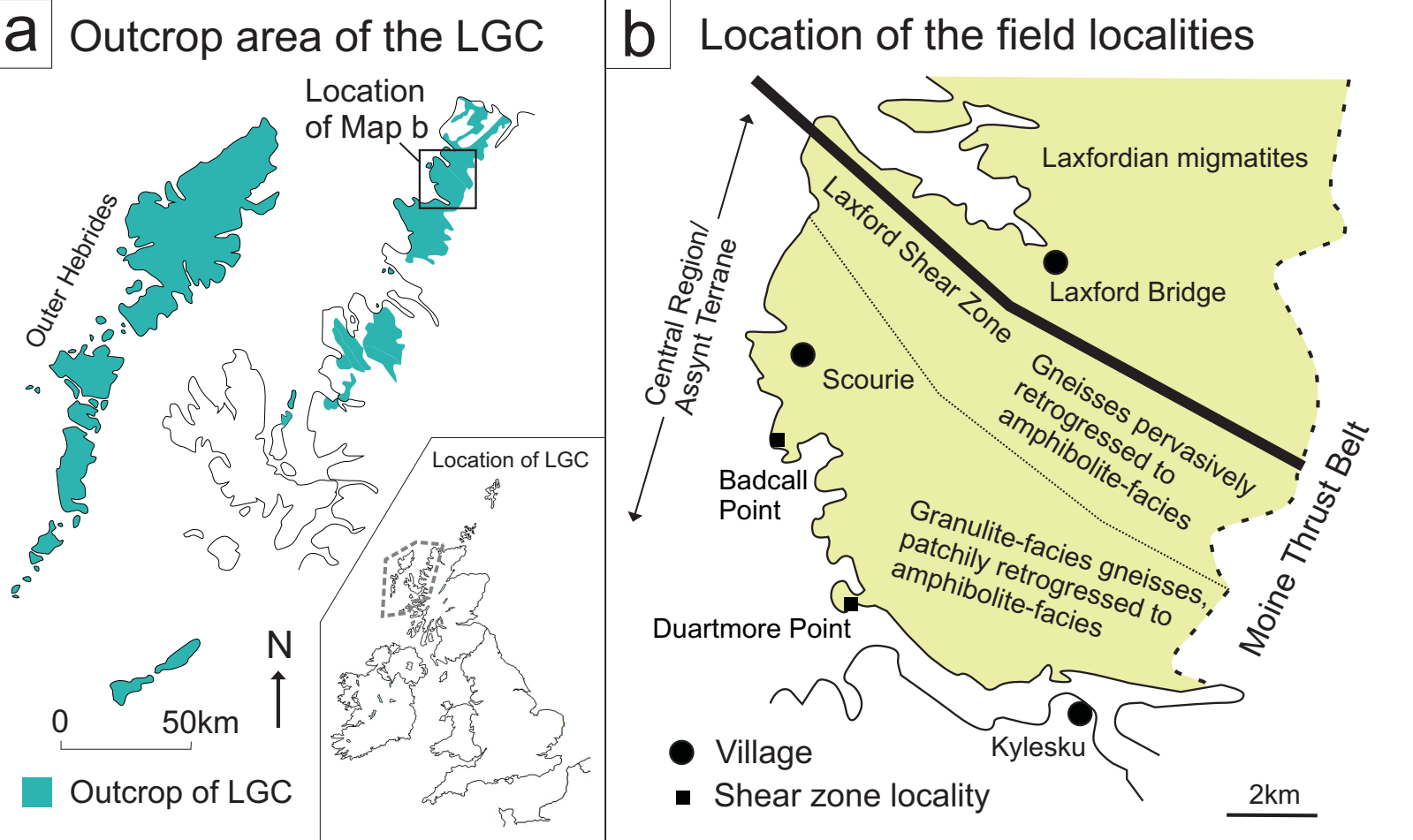
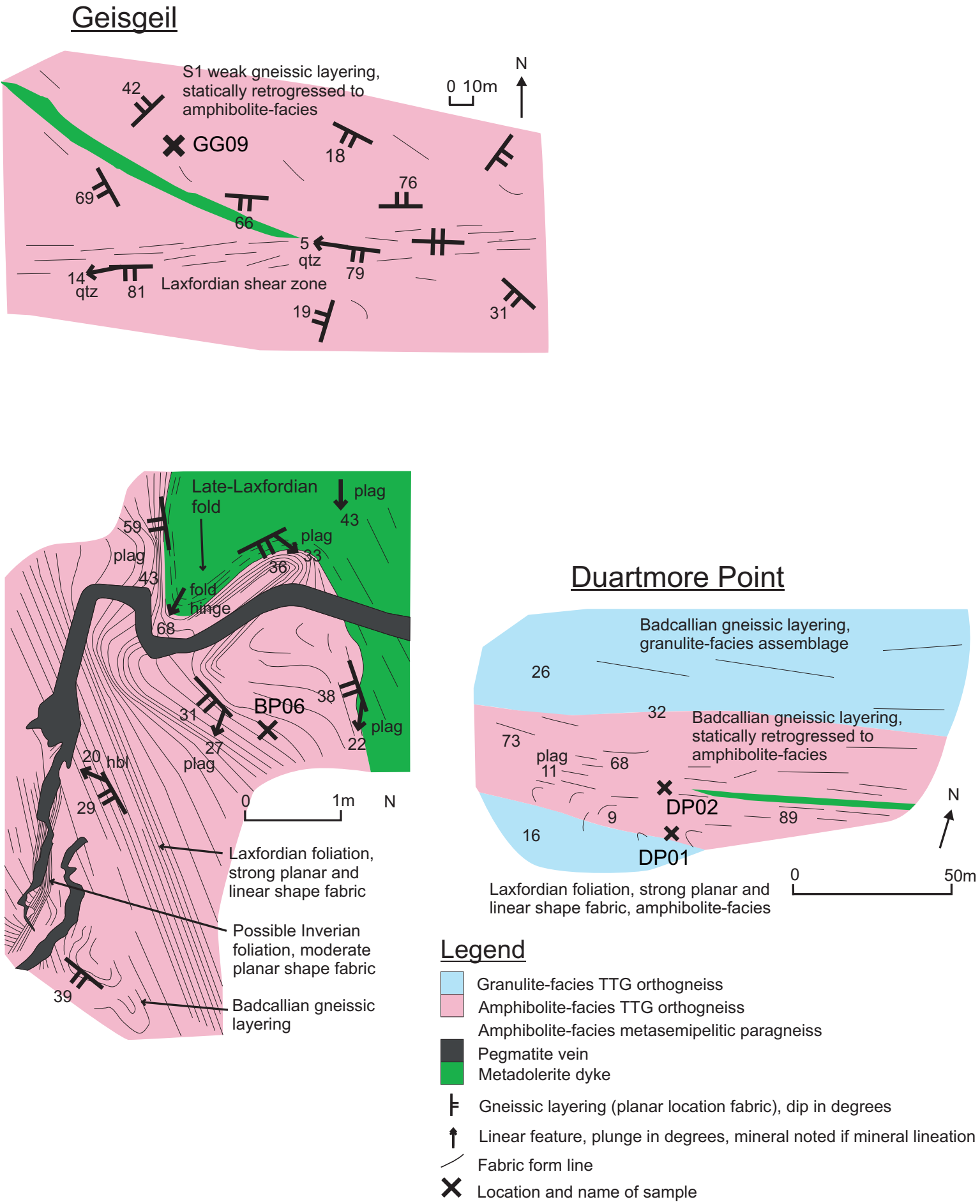


Figure
Click here to download Figure: Fig. 2.eps



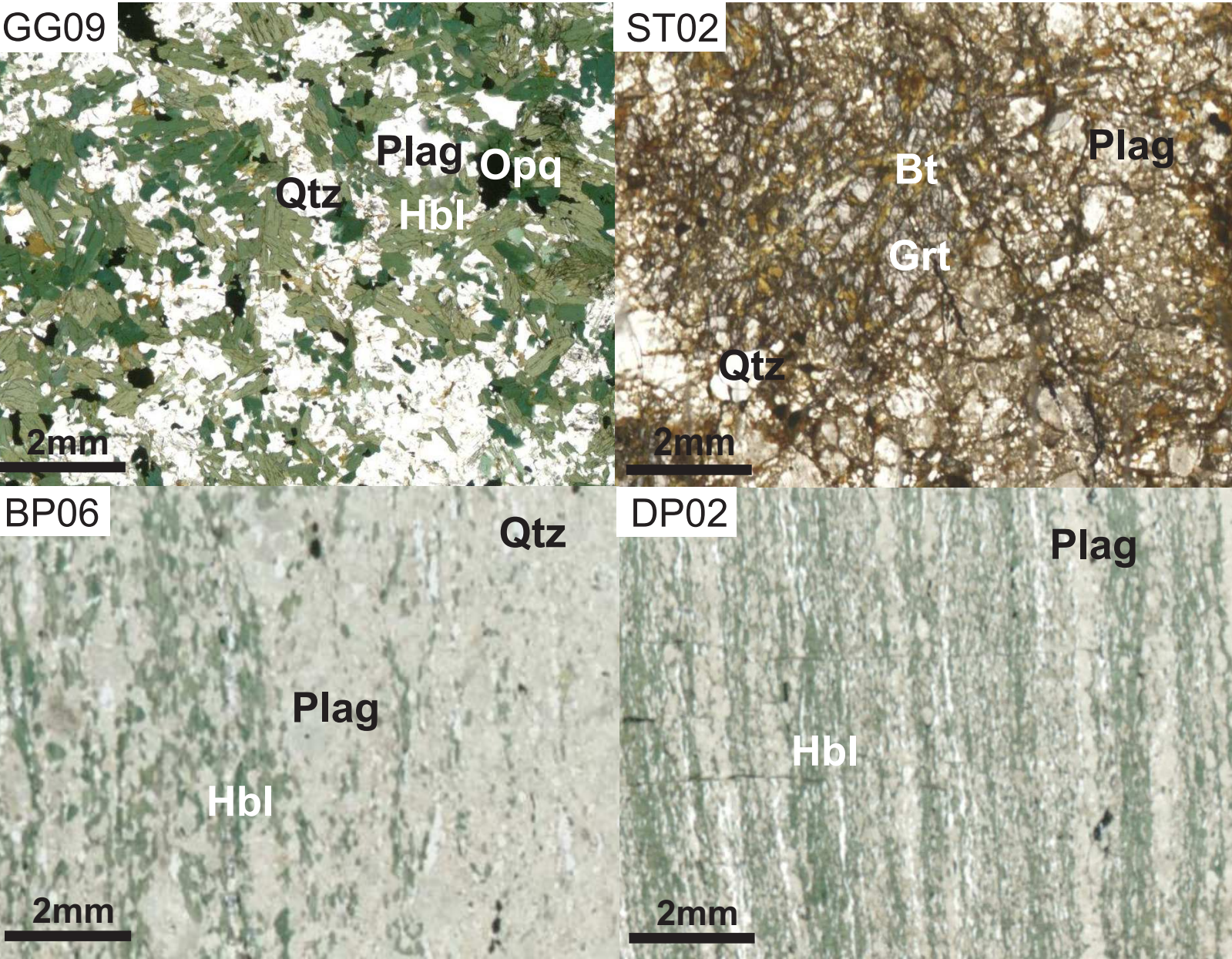
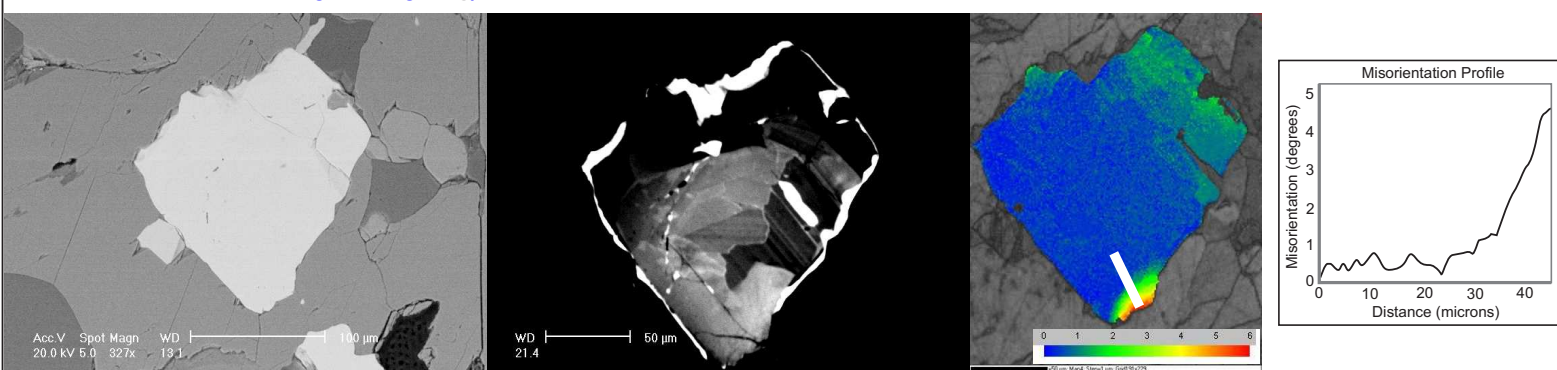
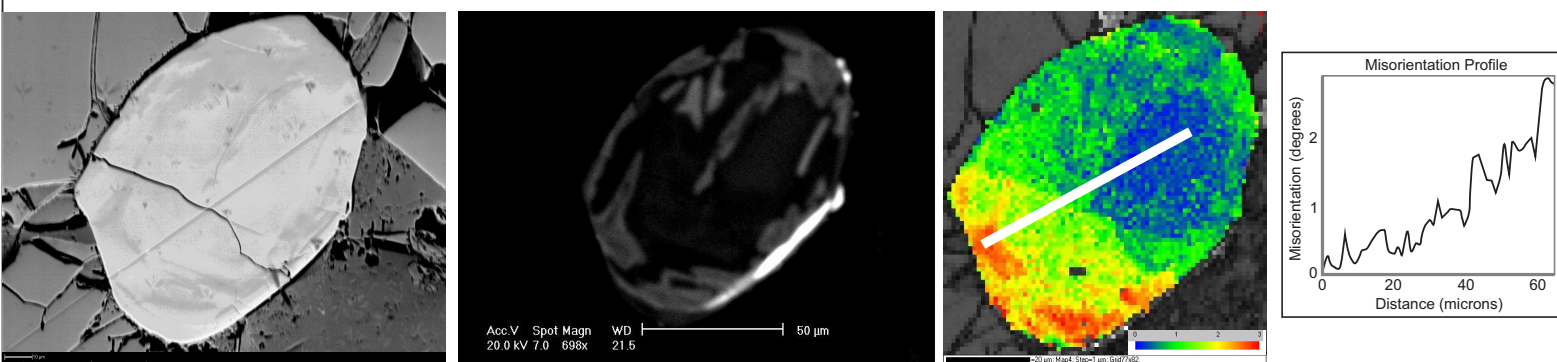


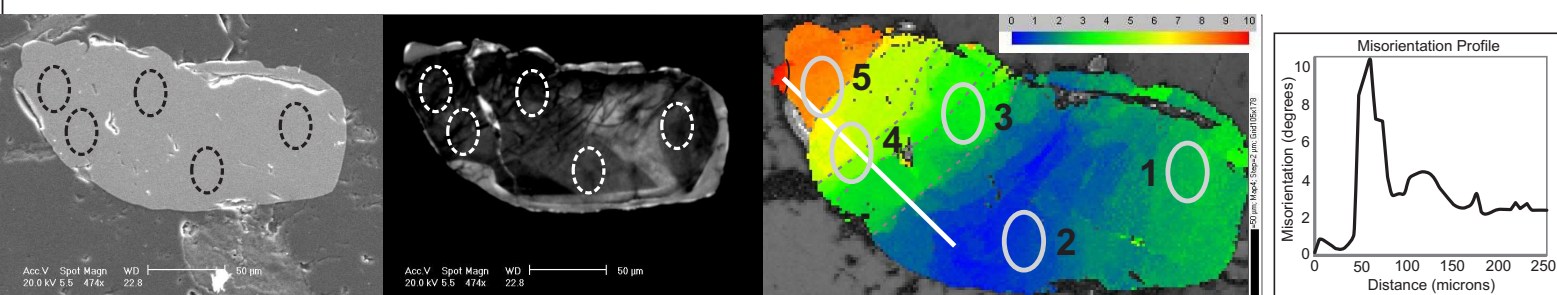
Figure
[Click here to download Figure. Fig. 419ps](#)
a: Zircon GG09/1. Left-right: BSE, CL, Texture Component map, Misorientation Profile



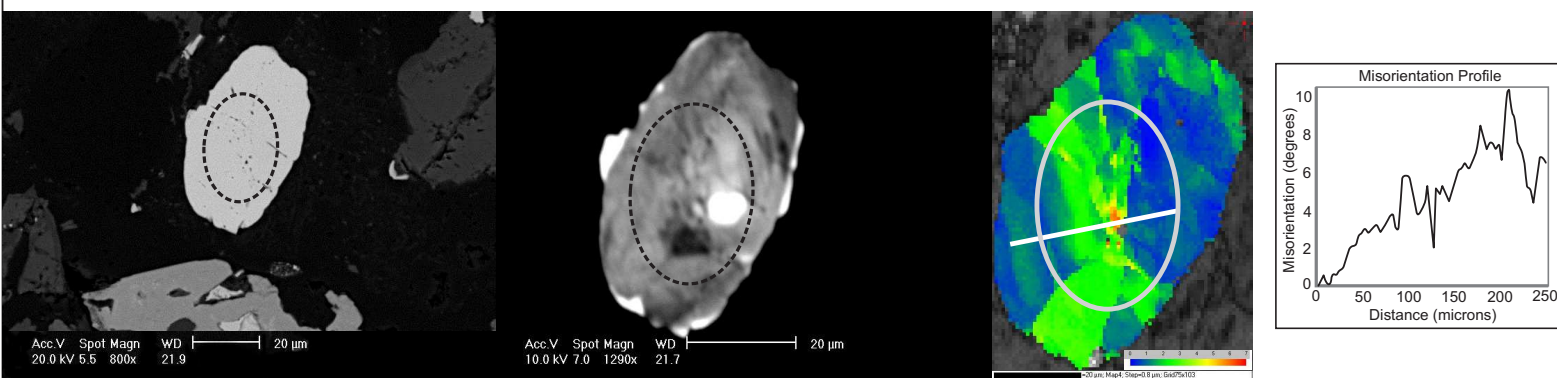
b: Zircon ST02/2. Left-right: BSE, CL, Texture Component map, Misorientation Profile



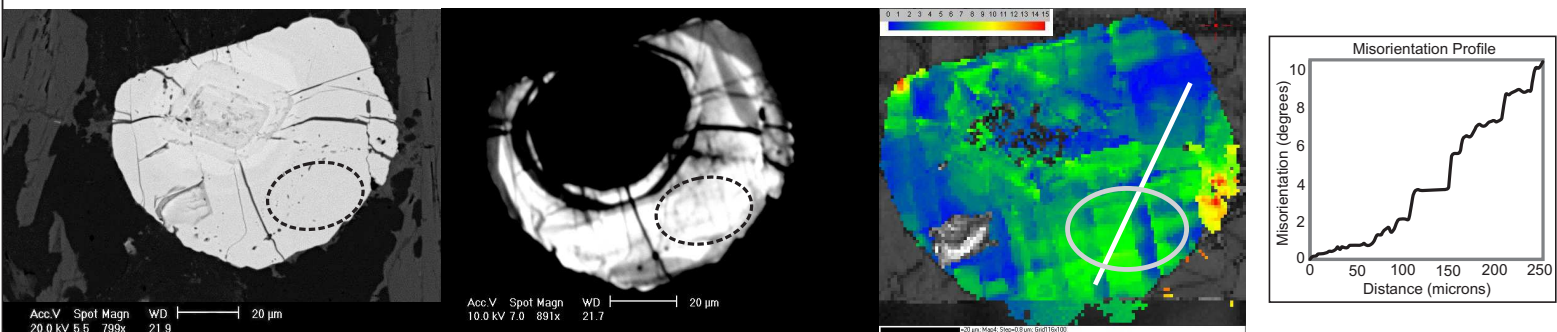
c: Zircon BP06/3. Left-right: BSE, CL, Texture Component map, Misorientation Profile



d: Zircon DP02/2. Left-right: BSE, CL, Texture Component map, Misorientation Profile



e: Zircon DP02/7. Left-right: BSE, CL, Texture Component map, Misorientation Profile



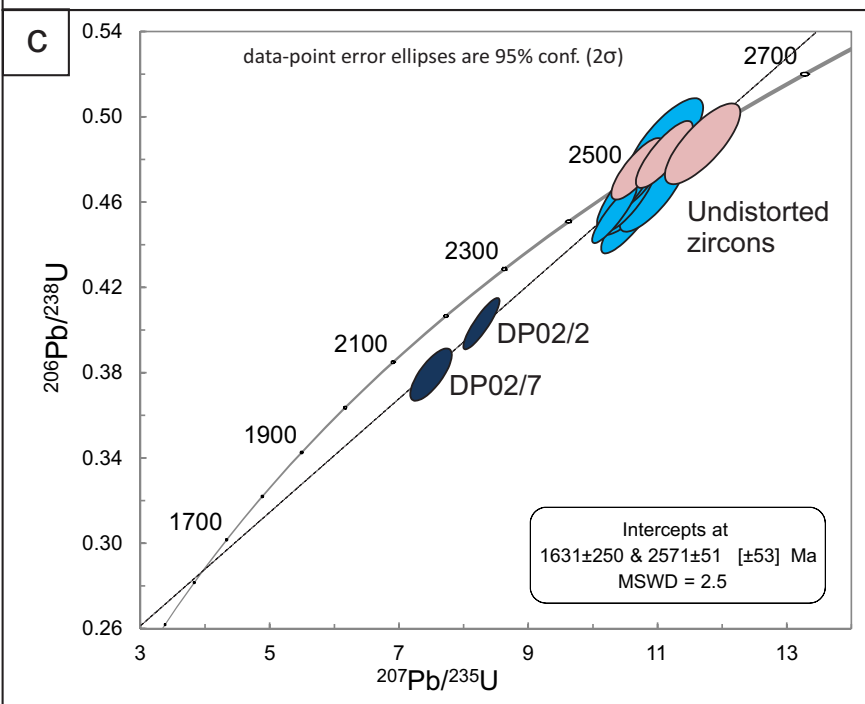
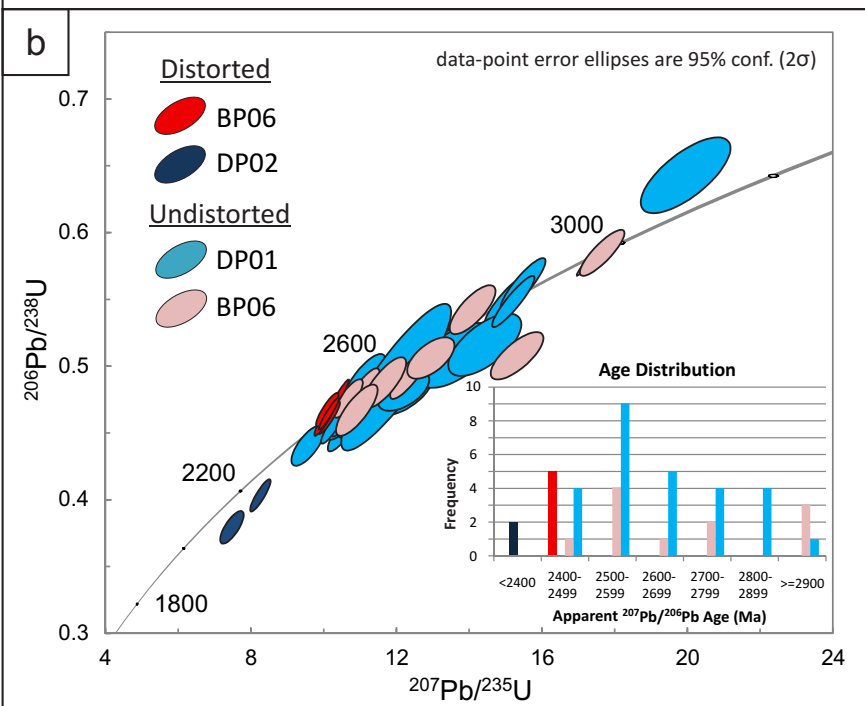
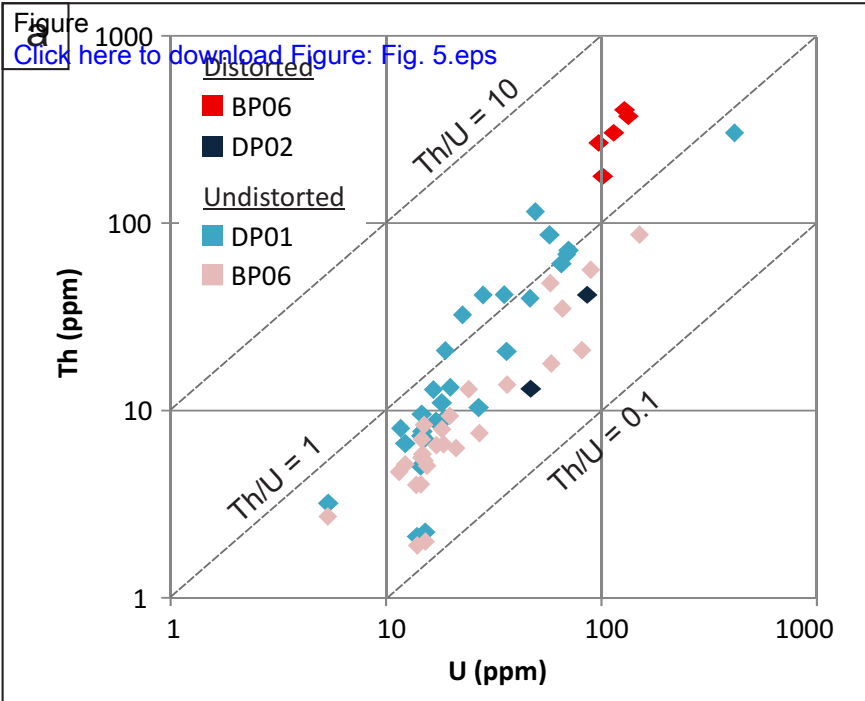


Figure
[Click here to download Figure: Fig. 6.eps](#)

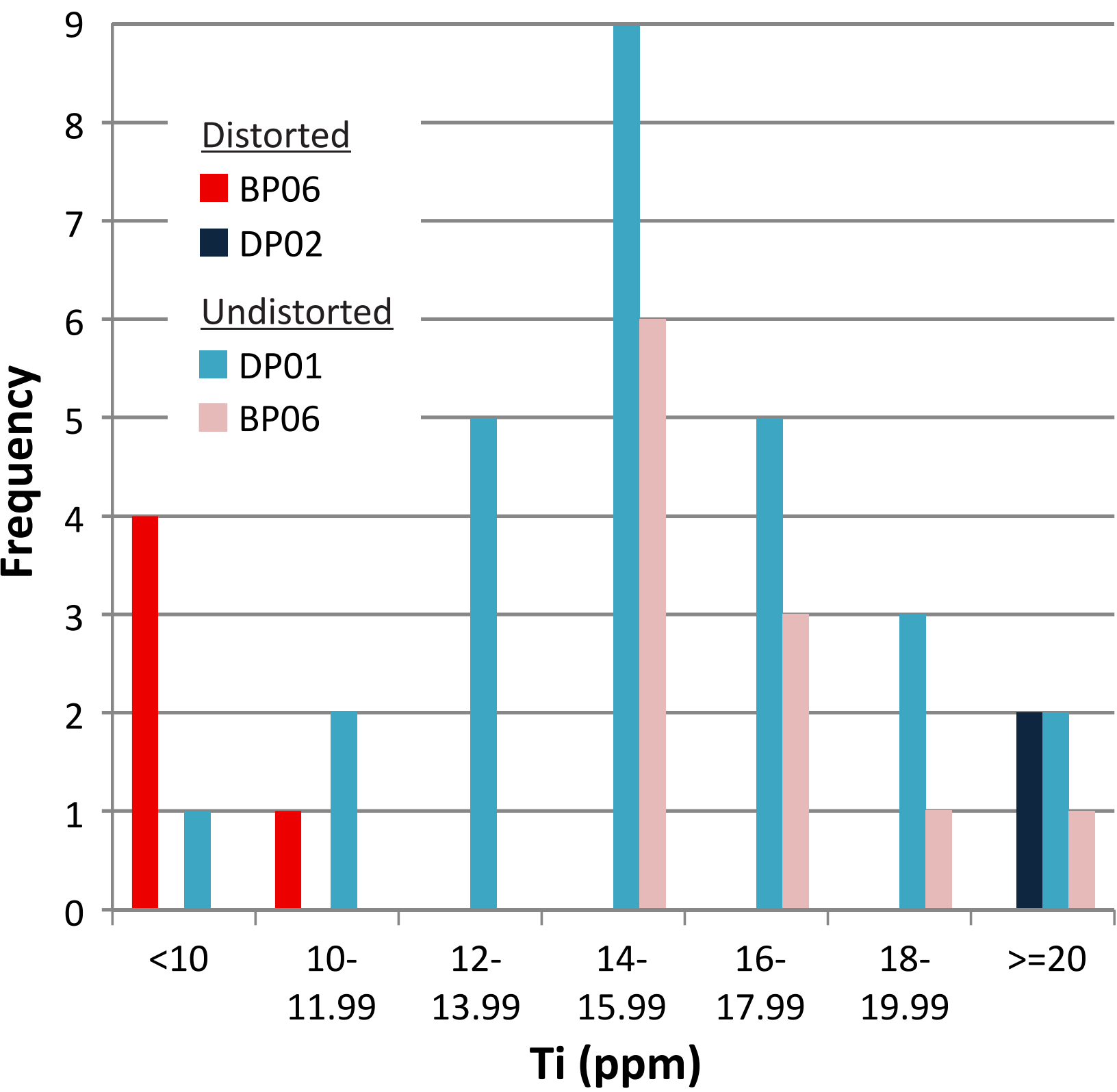
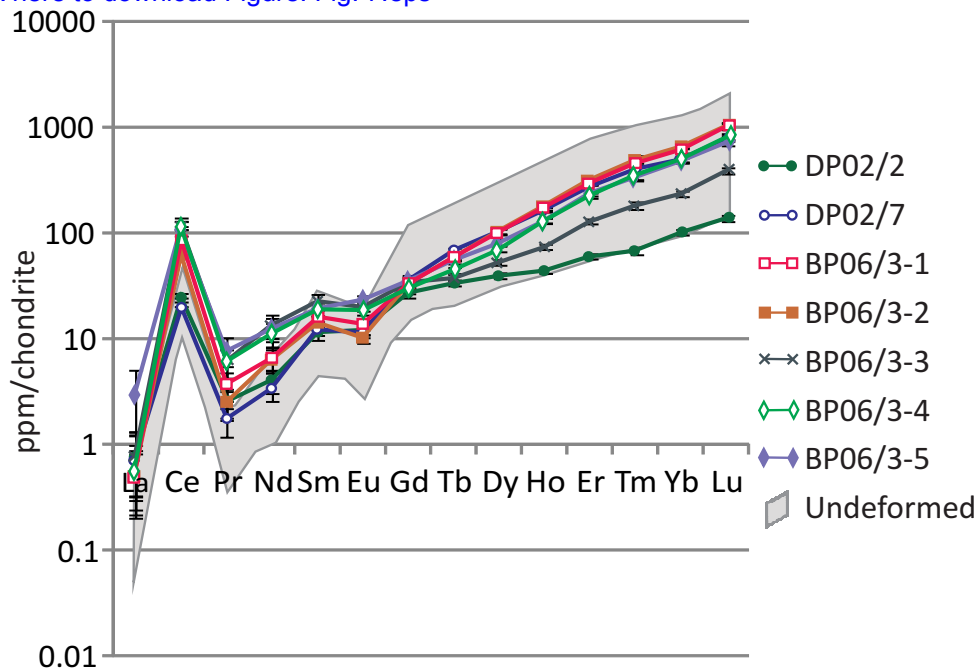
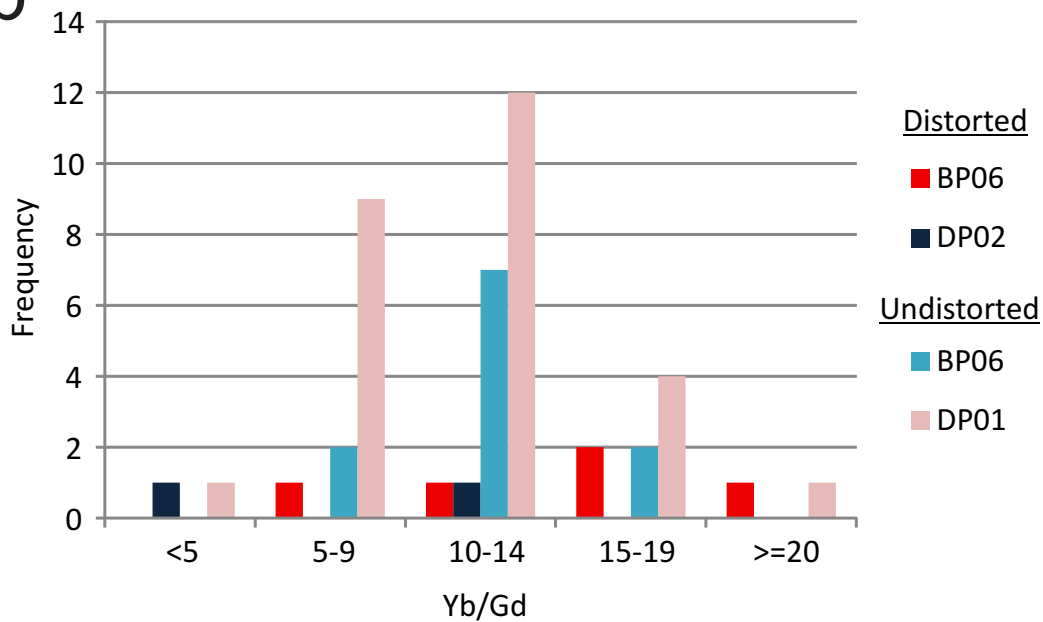


Figure
[Click here to download Figure: Fig. 7.eps](#)



b



c

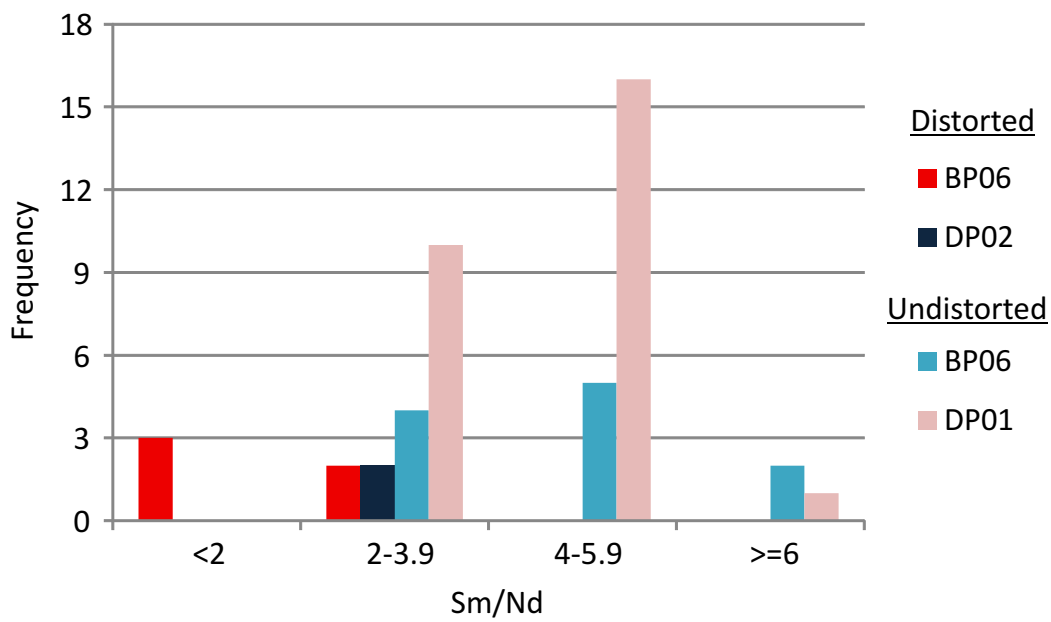


Figure
[Click here to download Figure: Fig. 8.eps](#)

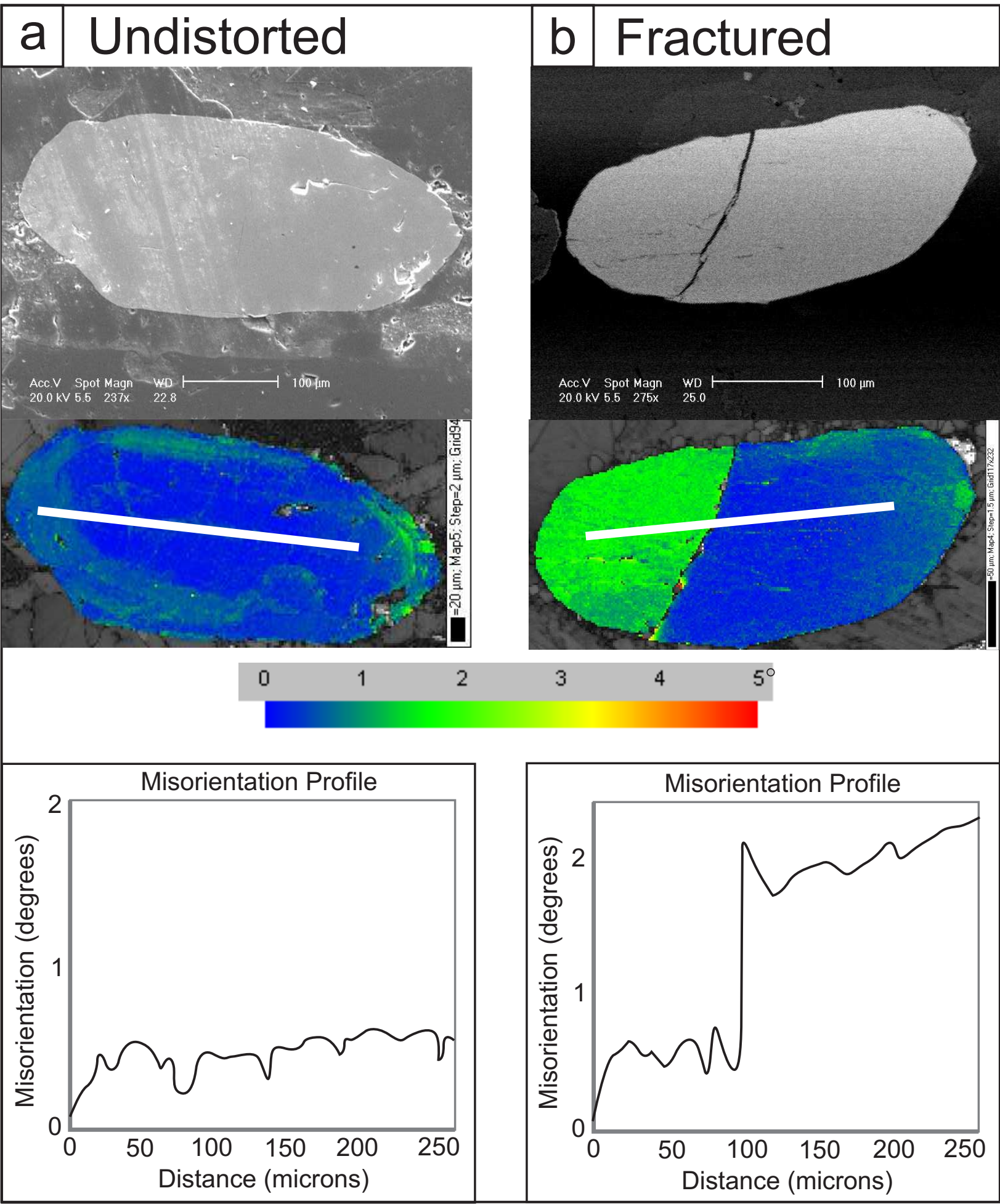
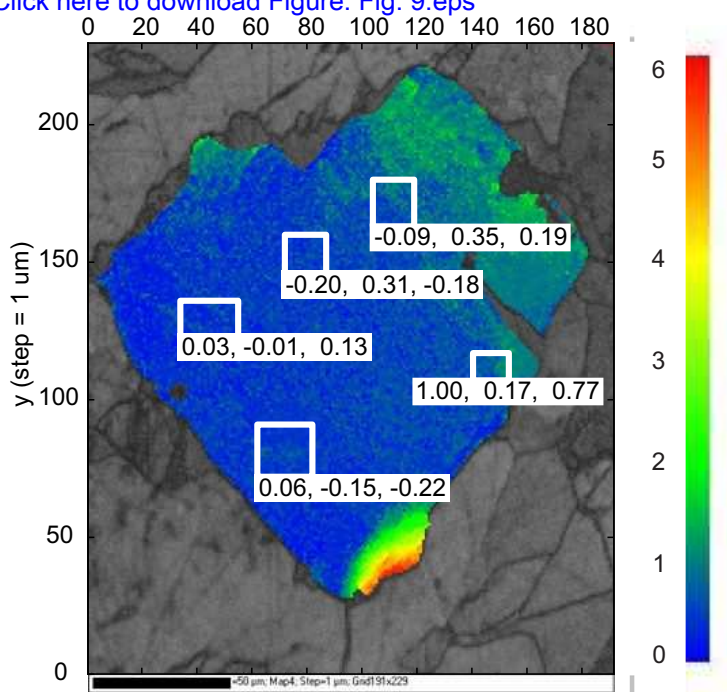
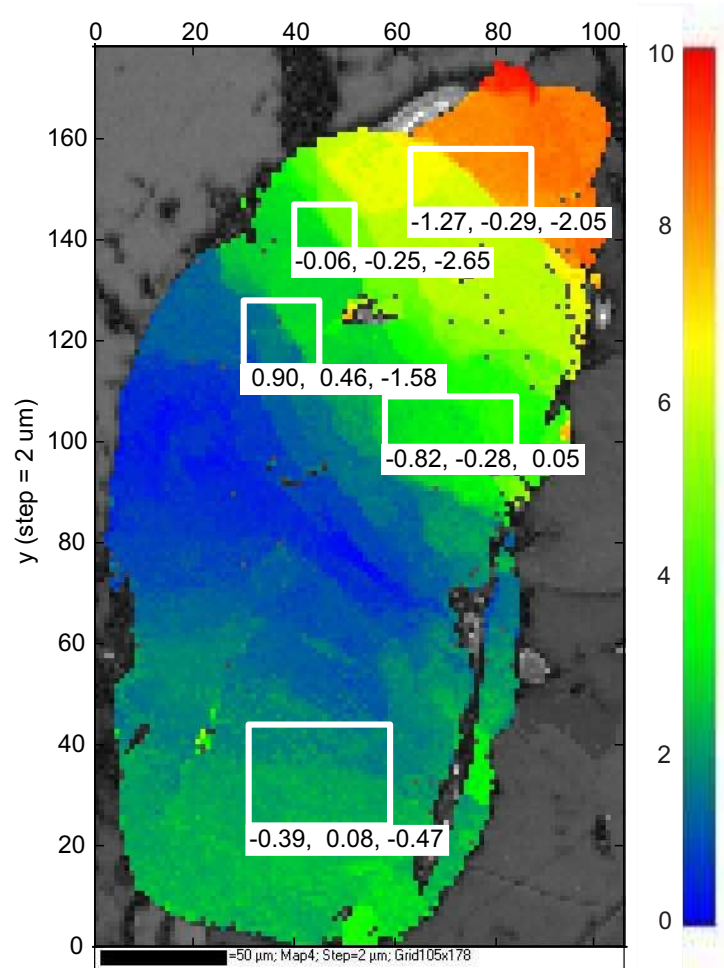


Figure
[Click here to download Figure: Fig. 9.eps](#)

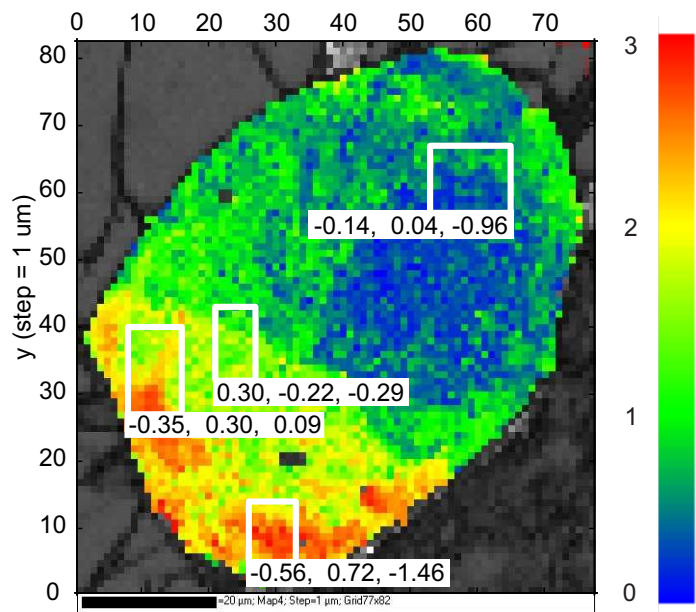
GG09/1



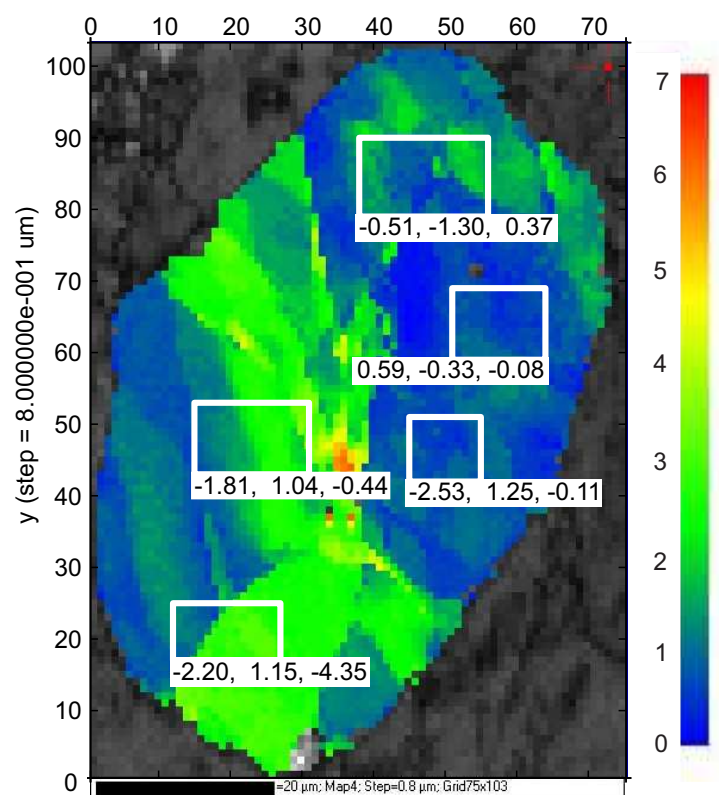
BP06/3



ST02/2



DP02/2



DP02/7

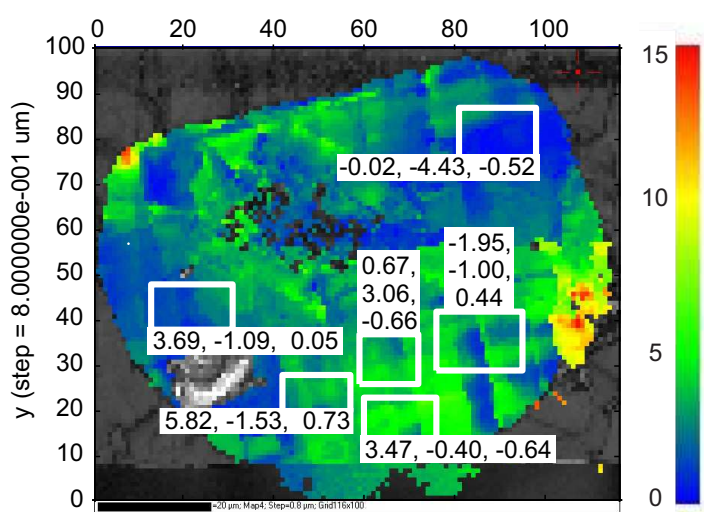


Table 1

Analysis ID	U (ppm)	Th (ppm)	Th/U	²⁰⁴ Pb _c (ppb)	²⁰⁷ Pb/ ²⁰⁶ Pb	2σ	²⁰⁷ Pb/ ²³⁵ U	2σ	²⁰⁶ Pb/ ²³⁸ U	2σ	Error Corr.	% Disc.	²⁰⁷ Pb/ ²⁰⁶ Pb Age	2σ
<u>Distorted Zircons</u>														
BP06/3-1	97.1	267.5	2.82	7.3	0.160	0.002	10.170	0.237	0.462	0.010	0.915	0.26	2453	16
BP06/3-2	101.6	177.4	1.79	7.3	0.158	0.001	10.393	0.259	0.476	0.011	0.964	-3.02	2437	12
BP06/3-3	128.3	400.8	3.20	5.4	0.158	0.001	10.054	0.243	0.461	0.010	0.927	-0.24	2437	14
BP06/3-4	114.3	302.7	2.72	5.8	0.157	0.002	10.113	0.252	0.468	0.010	0.881	-2.10	2422	20
BP06/3-5	133.5	370.5	2.85	5.2	0.159	0.001	10.159	0.225	0.465	0.010	0.947	-0.84	2440	12
DP02/2-1	86.1	41.3	0.49	7.8	0.149	0.002	8.271	0.229	0.403	0.010	0.883	6.28	2331	22
DP02/7-1	47.1	13.0	0.28	5.8	0.143	0.003	7.491	0.263	0.379	0.010	0.751	8.49	2266	40
<u>Undistorted Zircons</u>														
BP06/1-1	49.5	38.4	0.80	2.5	0.170	0.003	10.953	0.333	0.468	0.012	0.810	3.09	2554	30
BP06/1-2	421.3	294.9	0.72	0.0	0.217	0.001	17.415	0.365	0.583	0.012	0.977	-0.12	2956	8
BP06/2-1	72.8	66.1	0.93	2.6	0.219	0.003	17.668	0.500	0.585	0.014	0.850	0.12	2973	24
GMBP06/1-2	20.4	20.2	1.01	1.0	0.182	0.003	12.399	0.456	0.495	0.016	0.858	2.87	2668	32
GMBP06/2-1	24.4	31.3	1.32	1.5	0.167	0.003	11.107	0.360	0.483	0.013	0.820	-0.54	2526	30
GMBP06/2-2	30.2	40.0	1.36	0.1	0.189	0.004	14.106	0.514	0.543	0.015	0.757	-2.38	2729	40
GMBP06/3-1	18.0	12.5	0.71	0.0	0.174	0.004	11.699	0.477	0.488	0.015	0.778	1.29	2595	42
GMBP06/3-2	21.5	12.9	0.61	2.7	0.163	0.003	10.688	0.329	0.476	0.012	0.808	-1.01	2485	30
GMBP06/5-1	12.8	7.8	0.62	2.5	0.170	0.004	10.923	0.467	0.467	0.016	0.785	3.14	2552	44
GMBP06/5-2	52.4	111.5	2.18	1.2	0.186	0.006	12.960	0.532	0.506	0.013	0.609	2.29	2703	54
GMBP06/6-1	37.8	40.1	1.09	1.5	0.219	0.006	15.330	0.592	0.508	0.015	0.741	10.90	2972	42
DP01/4-1	15.3	2.2	0.15	0.0	0.166	0.004	10.629	0.369	0.463	0.013	0.788	2.74	2522	36
DP01/4-2	14.0	2.1	0.16	0.7	0.188	0.006	13.338	0.541	0.514	0.014	0.664	1.82	2725	48
DP01/6-1	18.3	11.0	0.62	0.3	0.169	0.003	10.605	0.390	0.454	0.014	0.866	5.39	2551	30
DP01/6-2	17.2	8.8	0.52	0.6	0.166	0.004	10.734	0.417	0.468	0.014	0.793	1.83	2521	38
DP01/6-3	58.0	87.2	1.54	0.3	0.166	0.004	10.556	0.359	0.460	0.012	0.780	3.21	2521	36
DP01/6-4	14.7	9.6	0.67	0.0	0.177	0.005	11.725	0.515	0.480	0.015	0.733	3.67	2625	50

Table 1 (cont.)

Analysis ID	U (ppm)	Th (ppm)	Th/U	²⁰⁴ Pb _c (ppb)	²⁰⁷ Pb/ ²⁰⁶ Pb	2σ	²⁰⁷ Pb/ ²³⁵ U	2σ	²⁰⁶ Pb/ ²³⁸ U	2σ	Error Corr.	% Disc.	²⁰⁷ Pb/ ²⁰⁶ Pb Age	2σ
<u>Undistorted Zircons (cont.)</u>														
DP01/6-5	18.6	8.9	0.49	1.3	0.171	0.004	10.911	0.407	0.463	0.014	0.797	4.30	2565	36
DP01/10-1	13.9	5.0	0.37	1.7	0.178	0.007	11.415	0.536	0.465	0.014	0.625	6.53	2634	60
DP01/10-2	14.5	5.1	0.36	0.8	0.184	0.008	12.208	0.677	0.482	0.015	0.574	5.50	2685	74
DP01/10-3	15.5	6.6	0.43	4.9	0.158	0.004	9.575	0.368	0.441	0.012	0.725	3.14	2430	44
GMDP01/1-1	36.5	20.8	0.58	1.3	0.167	0.002	10.596	0.298	0.461	0.011	0.885	3.05	2523	22
GMDP01/1-2	27.2	10.4	0.39	1.1	0.164	0.003	10.677	0.341	0.471	0.012	0.800	0.59	2502	32
GMDP01/2-1	15.1	11.7	0.80	0.0	0.225	0.008	19.960	1.007	0.643	0.023	0.715	-6.12	3017	56
GMDP01/2-2	89.1	105.4	1.21	2.3	0.163	0.001	10.372	0.264	0.463	0.011	0.942	1.23	2482	14
GMDP01/2-4	149.9	173.2	1.19	2.2	0.192	0.002	13.849	0.360	0.524	0.013	0.952	1.59	2758	12
GMDP01/2-5	21.2	8.4	0.41	0.3	0.187	0.006	13.130	0.580	0.509	0.016	0.710	2.42	2717	52
GMDP01/3-1	15.1	7.1	0.48	0.7	0.194	0.010	13.629	0.898	0.508	0.020	0.594	4.71	2780	86
GMDP01/4-1	14.8	7.8	0.54	1.5	0.164	0.003	10.532	0.381	0.467	0.015	0.876	1.01	2494	28
GMDP01/4-2	12.3	6.7	0.56	1.0	0.165	0.004	11.116	0.482	0.489	0.017	0.782	-2.41	2506	44
GMDP01/5-1	81.0	33.8	0.43	5.6	0.198	0.002	14.929	0.398	0.548	0.013	0.916	-0.44	2805	18
GMDP01/5-2	11.6	6.0	0.53	0.3	0.168	0.004	10.783	0.389	0.464	0.011	0.673	3.29	2542	44
GMDP01/6-1	5.4	3.2	0.61	1.1	0.203	0.009	14.440	0.822	0.516	0.019	0.651	5.83	2849	70
GMDP01/6-2	24.2	19.4	0.82	1.1	0.200	0.003	15.491	0.506	0.561	0.016	0.882	-1.60	2827	24
GMDP01/6-3	65.7	61.0	0.95	2.4	0.201	0.003	15.229	0.475	0.549	0.016	0.916	0.58	2836	20
GMDP01/7-1	14.7	7.4	0.52	1.0	0.177	0.008	12.006	1.237	0.492	0.045	0.887	1.71	2624	78
GMDP01/8-1	19.8	13.3	0.69	0.9	0.184	0.007	12.209	0.578	0.482	0.012	0.542	5.59	2686	66
GMDP01/9-3	58.5	27.9	0.49	1.3	0.164	0.002	10.285	0.281	0.456	0.011	0.898	2.88	2493	20

Table 2

Analysis ID	La	Ce	Pr	Nd	Sm	Eu	Gd	Tb	Dy	Ho	Er	Tm	Yb	Lu	Sm/Nd	Yb/Gd	Ti	Ti Temp	2σ
<u>Distorted Zircons</u>																			
BP06ChZ3-1	0.51	85	3.65	6.56	16.1	13.4	33	57	102	172	296	448	597	1003	2.5	18	6.91	712	21
BP06ChZ3-2	0.55	68	2.42	6.26	14.3	10.0	33	58	104	182	316	491	656	1026	2.3	20	5.72	696	19
BP06ChZ3-3	0.83	125	6.00	13.32	22.7	20.0	34	38	52	73	128	180	233	383	1.7	7	6.19	703	20
BP06ChZ3-4	0.61	117	6.08	11.13	18.8	18.5	29	44	70	129	223	345	487	804	1.7	17	10.64	752	24
BP06ChZ3-5	3.12	117	7.82	12.41	19.2	23.2	36	54	81	131	234	335	479	708	1.5	13	8.10	727	22
DP02Z2-1	0.81	24	2.55	4.03	11.4	11.9	27	34	39	44	60	67	101	137	2.8	4	20.83	820	32
DP02Z7-1	0.75	22	1.68	3.39	12.6	11.3	35	67	102	166	268	400	494	773	3.7	14	46.56	914	44
<u>Undistorted Zircons</u>																			
BP06ChZ1-1	0.30	31	1.24	2.64	8.3	8.8	21	24	36	46	65	84	108	166	3.1	5	17.1	799	29
BP06ChZ1-2	0.46	47	1.57	5.18	21.0	19.2	62	104	180	298	516	814	1178	1977	4.0	19	14.6	783	27
BP06ChZ2-1	0.26	25	1.06	2.83	21.9	16.2	92	169	294	476	756	1012	1267	1750	7.7	14	15.8	791	28
GMBP06Z1-2	0.33	29	1.65	2.79	13.9	8.2	41	62	106	159	262	340	445	621	5.0	11	17.9	804	30
GMBP06Z2-1	0.28	39	1.84	7.05	20.4	13.1	60	97	168	272	386	508	647	1095	2.9	11	16.7	797	29
GMBP06Z2-2	0.16	39	1.46	5.09	27.4	18.7	113	183	298	456	676	890	1015	1678	5.4	9	18.8	809	30
GMBP06Z3-1	0.29	27	0.52	1.65	5.2	4.6	42	67	121	179	295	375	464	740	3.1	11	15.4	788	28
GMBP06Z3-2	0.06	24	0.87	1.63	10.5	4.9	36	57	105	156	270	375	393	698	6.4	11	14.8	784	28
GMBP06Z5-1	0.44	26	0.40	2.03	9.9	3.2	33	62	94	166	276	377	448	774	4.9	13	15.8	791	28
GMBP06Z5-2	0.28	43	0.72	2.95	12.7	5.7	70	112	212	365	565	861	1101	1764	4.3	16	14.6	783	27
GMBP06Z6-1	0.25	36	1.70	5.50	16.6	8.1	75	112	200	318	491	653	807	1222	3.0	11	23.7	834	33
DP01Z4-1	0.25	36	0.99	2.66	15.1	8.7	55	95	167	257	424	570	725	1074	5.7	13	17.8	803	30
DP01Z4-2	0.33	32	0.89	2.25	13.2	7.4	49	84	146	232	389	510	626	932	5.8	13	16.4	794	29
DP01Z6-1	0.58	29	1.80	4.10	16.8	12.6	53	73	118	181	277	365	446	671	4.1	8	17.1	799	29
DP01Z6-2	0.35	28	1.51	4.11	15.7	12.4	47	74	114	167	262	363	435	648	3.8	9	15.9	791	28
DP01Z6-3	0.36	31	1.03	2.49	9.5	7.1	24	32	53	75	101	137	160	253	3.8	7	15.1	786	28
DP01Z6-4	0.47	26	1.82	3.03	14.7	12.9	40	60	95	142	220	304	377	548	4.9	9	17.8	803	30

Table 2 (cont.)

Analysis ID	La	Ce	Pr	Nd	Sm	Eu	Gd	Tb	Dy	Ho	Er	Tm	Yb	Lu	Sm/Nd	Yb/Gd	Ti	Ti Temp	2 σ
<u>Undistorted Zircons (cont.)</u>																			
DP01Z6-5	0.61	27	1.53	4.18	16.5	14.3	48	72	114	172	253	355	453	624	3.9	9	18.6	808	30
DP01Z10-1	0.83	32	2.10	4.01	15.1	16.8	40	62	97	142	219	280	373	540	3.8	9	20.3	817	31
DP01Z10-2	0.38	26	1.35	3.44	13.5	9.8	40	60	98	150	221	319	393	565	3.9	10	19.8	814	31
DP01Z10-3	0.14	24	1.20	2.30	11.1	9.5	29	44	69	113	169	222	280	403	4.8	10	15.8	790	28
GMDP01Z1-1	0.29	27	0.78	1.18	7.4	4.7	28	50	82	132	222	342	436	690	6.3	16	13.3	774	26
GMDP01Z1-2	0.21	27	0.98	1.59	8.1	7.5	23	46	83	135	232	341	467	698	5.1	20	8.3	729	22
GMDP01Z2-1	0.28	21	0.89	2.29	10.8	8.5	33	51	82	121	186	256	339	475	4.7	10	14.9	785	28
GMDP01Z2-2	0.25	25	0.90	1.48	5.8	6.3	17	30	47	68	112	154	206	305	3.9	12	14.9	785	28
GMDP01Z2-4	0.30	28	1.08	3.06	16.5	16.5	50	69	94	110	131	141	165	181	5.4	3	14.1	780	27
GMDP01Z2-5	0.28	20	1.16	2.10	9.2	7.7	28	45	72	110	172	246	309	491	4.4	11	15.1	786	28
GMDP01Z3-1	0.55	25	1.74	3.68	14.7	13.2	46	79	118	185	289	372	478	714	4.0	10	20.8	819	32
GMDP01Z4-1	0.24	27	1.58	3.69	12.9	10.7	36	55	88	132	199	270	334	464	3.5	9	10.0	745	24
GMDP01Z4-2	0.50	26	1.92	3.51	15.3	12.8	43	58	93	139	217	293	379	534	4.4	9	12.8	769	26
GMDP01Z5-1	0.47	15	0.62	2.04	8.0	9.6	28	44	72	108	175	241	303	491	3.9	11	10.8	753	24
GMDP01Z5-2	0.35	21	1.17	2.53	8.1	5.6	23	36	56	85	133	166	223	338	3.2	10	17.2	800	29
GMDP01Z6-1	0.14	24	0.72	1.98	10.0	7.4	29	50	86	137	219	312	429	599	5.0	15	13.7	776	27
GMDP01Z6-2	0.26	21	0.76	1.55	7.9	8.5	29	47	81	135	225	322	434	645	5.1	15	14.2	780	27
GMDP01Z6-3	0.29	25	0.80	1.88	8.0	8.2	26	44	71	114	186	272	379	583	4.3	14	13.9	778	27
GMDP01Z7-1	0.40	25	1.55	3.89	12.4	12.1	40	65	98	149	238	309	391	569	3.2	10	19.3	812	31
GMDP01Z8-1	0.22	25	0.73	2.12	11.5	8.7	34	59	105	173	281	387	532	846	5.4	16	15.3	788	28
GMDP01Z9-3	0.08	26	1.05	1.92	10.3	7.3	27	42	59	85	125	159	213	293	5.4	8	13.4	774	27

Table 3

Zircon	Distortion Pattern	CL	Th/U	²⁰⁷ Pb/ ²⁰⁶ Pb Age (Ma)	Ti	REE Pattern
Zircon GG09/1 from sample GG09 from Geisgeil	Bending at one corner of the grain	Narrow very bright rim, dark and light zones partially overprinting earlier oscillatory zoning. Two narrow dark lines pass through the area of plastic distortion but do not appear related to the microstructure	-	-	-	-
Zircon ST02/2 from sample ST02 from Sithean Mor	Fairly gentle lattice bending across the crystal	Generally quite dark with some irregular lighter patches unrelated to microstructure	-	-	-	-
Zircon BP06/3-1 from sample BP06 from Badcall Point	Lattice bent in one half of the crystal into a series of subgrains	Generally quite dark with patchy slightly brighter rim, low density of sinuous dark lines	2.8 - much higher than zircons without lattice distortion	2453±16Ma - concordant but slightly younger than youngest ages from zircons without lattice distortion	6.9ppm - well below the main cluster of Ti concentrations	Typical zircon pattern
Zircon BP06/3-2 from sample BP06 from Badcall Point	Lattice bent in one half of the crystal into a series of subgrains	As BP06ChZ3-1	1.8 - higher than zircons without lattice distortion	2437±12Ma - concordant but slightly younger than youngest ages from zircons without lattice distortion	5.7ppm - well below the main cluster of Ti concentrations	Typical zircon pattern
Zircon BP06/3-3 from sample BP06 from Badcall Point	Lattice bent in one half of the crystal into a series of subgrains	As BP06ChZ3-1 but with a high density of sinuous black lines	3.2 - about 3x higher than zircons without lattice distortion	2437±14Ma - concordant but slightly younger than youngest ages from zircons without lattice distortion	6.2ppm - well below the main cluster of Ti concentrations	Relatively depleted in heavy REE (Yb/Gd = 7)
Zircon BP06/3-4 from sample BP06 from Badcall Point	Lattice bent in one half of the crystal into a series of subgrains	As BP06ChZ3-1, this spot covers some of the brighter rim	2.7 - much higher than zircons without lattice distortion	2422±20Ma - concordant but slightly younger than youngest ages from zircons without lattice distortion	10.6ppm - below the main cluster of Ti concentrations	Typical zircon pattern
Zircon BP06/3-5 from sample BP06 from Badcall Point	Lattice bent in one half of the crystal into a series of subgrains	As BP06ChZ3-1 but with a high density of sinuous black lines	2.9 - much higher than zircons without lattice distortion	2440±12Ma - concordant but slightly younger than youngest ages from zircons without lattice distortion	8.1ppm - well below the main cluster of Ti concentrations	Typical zircon pattern
Zircon DP02/2 from sample DP02 from Duartmore Point	Folded pattern across crystal with possibly patchy development of subgrain walls	Medium grey emittance, very bright spot near centre, some irregular dark lines possibly related to microstructure	0.5 - within range of zircons without lattice distortion but below average	2331±22Ma – 6.3% discordance, likely due to Pb-loss during the Laxfordian tectonothermal event, enabled by earlier lattice distortion	20.8ppm - at the higher end of Ti concentrations recorded by undistorted zircons	Relatively flat heavy REE pattern (Yb/Gd = 4)
Zircon DP02/7 from sample DP02 from Duartmore Point	Unusual cross-hatched pattern	Very dark core, very bright rim with dark fracture lines	0.3 - within range of zircons without lattice distortion but well below average	2266±40Ma – 8.5% discordance, likely due to Pb-loss during the Laxfordian tectonothermal event, enabled by earlier lattice distortion	46.6ppm – 25ppm higher than any other recorded Ti concentrations	Subdued Eu anomaly

Table 4

<u>Distorted Zircon</u>	<u>Sample from which undistorted comparison zircons were obtained</u>			
	<u>For U-Pb dating</u>	<u>For Th/U</u>	<u>For REEs</u>	<u>For Ti</u>
BP06/3	BP06 – same sample, and DP01 – records same age spectrum as BP06	BP06 – same sample	BP06 – same sample, and DP01 – records same compositional range as JM09/BP06	BP06 – same sample
DP02/2	BP06 – also a Laxfordian shear zone, located 6km away, interpreted to have underwent same tectonothermal history as DP02 , and DP01 – records same age spectrum as BP06	DP01 – located only one metre from DP02 . While the host rock is heterogeneous in composition, these zircons are the closest geographically and are interpreted to offer the best comparison of trace element chemistry	DP01 – located only one metre from DP02 . While the host rock is heterogeneous in composition, these zircons are the closest geographically and are interpreted to offer the best comparison of trace element chemistry, and BP06 – records same compositional range as DP01	DP01 – located only one metre from DP02 . While the host rock is heterogeneous in composition, these zircons are the closest geographically and are interpreted to offer the best comparison of trace element chemistry
DP02/7	BP06 – also a Laxfordian shear zone, located 6km away, interpreted to have underwent same tectonothermal history as DP02 , and DP01 – records same age spectrum as BP06	DP01 – located only one metre from DP02 . While the host rock is heterogeneous in composition, these zircons are the closest geographically and are interpreted to offer the best comparison of trace element chemistry	DP01 – located only one metre from DP02 . While the host rock is heterogeneous in composition, these zircons are the closest geographically and are interpreted to offer the best comparison of trace element chemistry, and BP06 – records same compositional range as DP01	DP01 – located only one metre from DP02 . While the host rock is heterogeneous in composition, these zircons are the closest geographically and are interpreted to offer the best comparison of trace element chemistry

Table 5

Zircon	WBV components (μm) ⁻²			Approx. Ion Microprobe Spot
	a	b	c	
DP02Z7	5.82	-1.53	0.73	
DP02Z7	0.67	3.06	-0.66	
DP02Z7	-1.54	2.29	0.28	
DP02Z7	3.69	-1.09	0.05	
DP02Z7	-1.95	-1.00	0.44	
DP02Z7	3.47	-0.40	-0.64	
BP06ChZ3	-0.39	0.08	-0.47	1
BP06ChZ3	0.90	0.46	-1.58	
BP06ChZ3	-0.06	-0.25	-2.65	4
BP06ChZ3	-0.82	-0.28	0.05	3
BP06ChZ3	-1.27	-0.29	-2.05	5
ST02Z2	-0.14	0.04	-0.96	
ST02Z2	-0.35	0.30	0.09	
ST02Z2	-0.56	0.72	-1.46	
ST02Z2	0.30	-0.22	-0.29	
DP02Z2	0.59	-0.33	-0.08	
DP02Z2	-2.53	1.25	-0.11	
DP02Z2	-2.20	1.15	-4.35	
DP02Z2	-1.81	1.04	-0.44	
DP02Z2	-0.51	-1.30	0.37	
GG09Z1	0.03	-0.01	0.13	
GG09Z1	-0.09	0.35	0.19	
GG09Z1	1.00	0.17	0.77	
GG09Z1	0.06	-0.15	-0.22	
GG09Z1	-0.20	0.31	-0.18	